Bioorganic Chemistry 109 (2021) 104684

Contents lists available at ScienceDirect

Bioorganic Chemistry

journal homepage: www.elsevier.com/locate/bioorg

Design and synthesis of new carbamates as inhibitors for fatty acid amide hydrolase and cholinesterases: Molecular dynamic, *in vitro* and *in vivo* studies

Mahdi Faal Maleki [a], Hamid Nadri [b], Mostafa Kianfar [c], Najmeh Edraki [d], Farhad Eisvand [c], Razieh Ghodsi [a,e], Seyed Ahmad Mohajeri [c], Farzin Hadizadeh [a,e,*]

[a] Department of Medicinal Chemistry, School of Pharmacy, Mashhad University of Medical Sciences, Mashhad, Iran
[b] Department of Medicinal Chemistry, Faculty of Pharmacy and Pharmaceutical Sciences Research Center, Shahid Sadoughi University of Medical Sciences, Yazd, Iran
[c] Department of Pharmacodynamics and Toxicology, School of Pharmacy, Mashhad University of Medical Sciences, Mashhad, Iran
[d] Medicinal and Natural Products Chemistry Research Center, Shiraz University of Medical Sciences, Shiraz, Iran
[e] Biotechnology Research Center, Pharmaceutical Technology Institute, Mashhad University of Medical Sciences, Mashhad, Iran

ARTICLE INFO

Keywords:
Fatty acid amide hydrolase
Acetylcholinesterase
Inhibitors
Alzheimer's disease

ABSTRACT

As anandamide (*N*-arachidonoylethanolamine, AEA) shows neuroprotective effects, the inhibition of its degradative enzyme, fatty acid amide hydrolase (FAAH) has been considered as a hopeful avenue for the treatment of neurodegenerative diseases, like Alzheimer's disease (AD). Memory loss, cognitive impairment and diminution of the cholinergic tone, due to the dying cholinergic neurons in the basal forebrain, are common hallmarks in patients with AD. By taking advantage of cholinesterase inhibitors (ChEIs), the degradation of acetylcholine (ACh) is decreased leading to enhanced cholinergic neurotransmission in the aforementioned region and ultimately improves the clinical condition of AD patients. In this work, new carbamates were designed as inhibitors of FAAH and cholinestrases (ChEs) (acetylcholinestrase (AChE), butyrylcholinestrase (BuChE)) inspired by the structure of the native substrates, structure of active sites and the SARs of the well-known inhibitors of these enzymes. All the designed compounds were synthesized using different reactions. All the target compounds were tested for their inhibitory activity against FAAH and ChEs by employing the Cayman assay kit and Elman method respectively. Generally, compounds possessing aminomethyl phenyl linker was more potent compared to their corresponding compounds possessing piperazinyl ethyl linker. The inhibitory potential of the compounds **3a-q** extended from 0.83 ± 0.03 μM (**3i**) to ˃100 μM (**3a**) for FAAH, 0.39 ± 0.02 μM (**3i**) to 24% inhibition in 113 ± 4.8 μM **(3b**) for AChE, and 1.8 ± 3.2 μM **(3i)** to 23.2 ± 0.2 μM **(3b)** for BuChE.

Compound **3i** a heptyl carbamate analog possessing 2-oxo-1,2-dihydroquinolin ring and aminomethyl phenyl linker showed the most inhibitory activity against three enzymes. Also, compound **3i** was investigated for memory improvement using the Morris water maze test in which the compound showed better memory improvement at 10 mg/kg compared to reference drug rivastigmine at 2.5 mg/kg. Molecular docking and molecular dynamic studies of compound **3i** into the enzymes displayed the possible interactions of key residues of the active sites with compound **3i**. Finally, kinetic study indicated that **3i** inhibits AChE through the mixed- mode mechanism and non-competitive inhibition mechanism was revealed for BuChE.

Abbreviations: AEA, *N*-arachidonoylethanolamine (anandamide); ChEs, cholinestrases; ChEsI, cholinestrases inhibitor; FAAH, fatty acid amide hydrolase; AD, Alzheimer's disease; AChE, acetylcholinesterase; BuChE, butyrylcholinesterase; ACh, acetylcholine; Aβ, amyloid-β; MAGL, monoacylglycerol lipase; IL-1β, interleukin-1β; IL-6, interlukin-6; TNF-α, tumour necrosis factor-α; NFTs, neurofibrillary tangles; MAPK, mitogen-activated protein kinase; MAFP, methyl arachidonyl fluorophosphonate; GSK-3 β, glycogen synthase kinase-3β; iNOS, inducible nitric oxide synthase; COX-2, cyclooxygenase-2; NO, nitric oxide; CT, Catalytic triad; MAC, membrane access channel; ABP, acyl chain-binding pocket; CP, cytosolic port; PAS, anionic site; OH, oxyanion hole; MOE, molecular operating environment; RMSDs, root-mean-square derivations; RMSF, root mean square fluctuation; Rg, radius of gyration; AMC, 7-amino-4-methylcoumarin; AMC-AA, 7-amino-4-methylcoumarin-arachidonamide; DTNB, 5,5-Dithiobis-(2-nitrobenzoic acid); AT, acetylthiocholine iodide; LD_{50}, median lethal dose.

* Corresponding author at: Department of Medicinal Chemistry, School of Pharmacy Mashhad University of Medical Sciences, Mashhad, Iran. Biotechnology Research Center, Pharmaceutical Technology Institute, Mashhad University of Medical Sciences, Mashhad, Iran.
E-mail address: hadizadehf@mums.ac.ir (F. Hadizadeh).

https://doi.org/10.1016/j.bioorg.2021.104684
Received 4 August 2020; Received in revised form 12 January 2021; Accepted 22 January 2021
Available online 2 February 2021

1. Introduction:

Alzheimer's disease, a neurodegenerative disorder associated with the deterioration of memory, learning skills and other cognitive processes, is known to be the main cause of dementia in the elderly and it is predicted that 115 million people will suffer from AD by 2050 [1]. Amyloid-β (Aβ) plaques originated from extraneuronal accumulation of Aβ peptides [2] and intraneuronal aggregation of deformed shapes of hyperphosphorylated tau protein are the main pathological hallmarks of AD [3]. Both of the aforementioned phenomena lead to neuronal loss and synapse dysfunction especially in the cholinergic pathways in the brain including the basal forebrain, hippocampus, and cerebral cortex which are in charge of learning capability, memory and other cognitive skills [4]. Not for the purpose of curing AD but for the purpose of elevating the ACh level in those regions of the brain affected by Aβ plaques, the FDA has approved the use of ChEI's like galantamine, donepezil and rivastigmine in recent decades.

Unfortunately, worldwide efforts over the past two decades to find a new drug to cure the disease and stop its progression have remained fruitless. Thus, there is an urgent need to explore new targets that can address the aforementioned issues. Long-term post-mortem studies of AD patients have also revealed considerable increases in the level of inflammatory mediators at the amyloid deposits including activated microglia and astrocytes as well as proinflammatory cytokines (inter interleukin-1β (IL-1β), interleukin-6 (IL-6) and tumor necrosis factor-α (TNF-α)) [5]. These proinflammatory mediators, released by microglia and astrocytes, may accelerate the vicious cycle and maybe the main factor in the progression of AD [6] (Fig. 1.). Indeed, microglia itself may create a positive feedback mechanism and play a pivotal role in the disease progression via expressing of Aβ and tau [7–11].

FAAH with amidase and esterase activity is a membrane-bound protein from the serine hydrolase family [12]. FAAH has the ability of hydrolyzing and thereby terminating a class of bioactive lipids namely oleamide, 2-arachidonoylglycerol (2-AG) and especially AEA. Regarding the endocannabinoid system pathways in the brain, the inhibition of FAAH may result in the higher concentration of AEA and consequently AEA shows its anti-inflammatory effects through the activation of cannabinoid receptors CB_1 and CB_2 located on neurons, microglia and astrocytes [1] (Fig. 1.). Briefly, as shown in Fig. 1. the activation of cannabinoid receptors (CB_1/CB_2) via elevated concentration of AEA resulting from FAAH inhibition might stop the several processes in AD progression including; production of IL-1β, IL-6 and TNF-α in microglia which after release, activate the production of neurofibrillary tangles (NFTs) in neurons through mitogen-activated

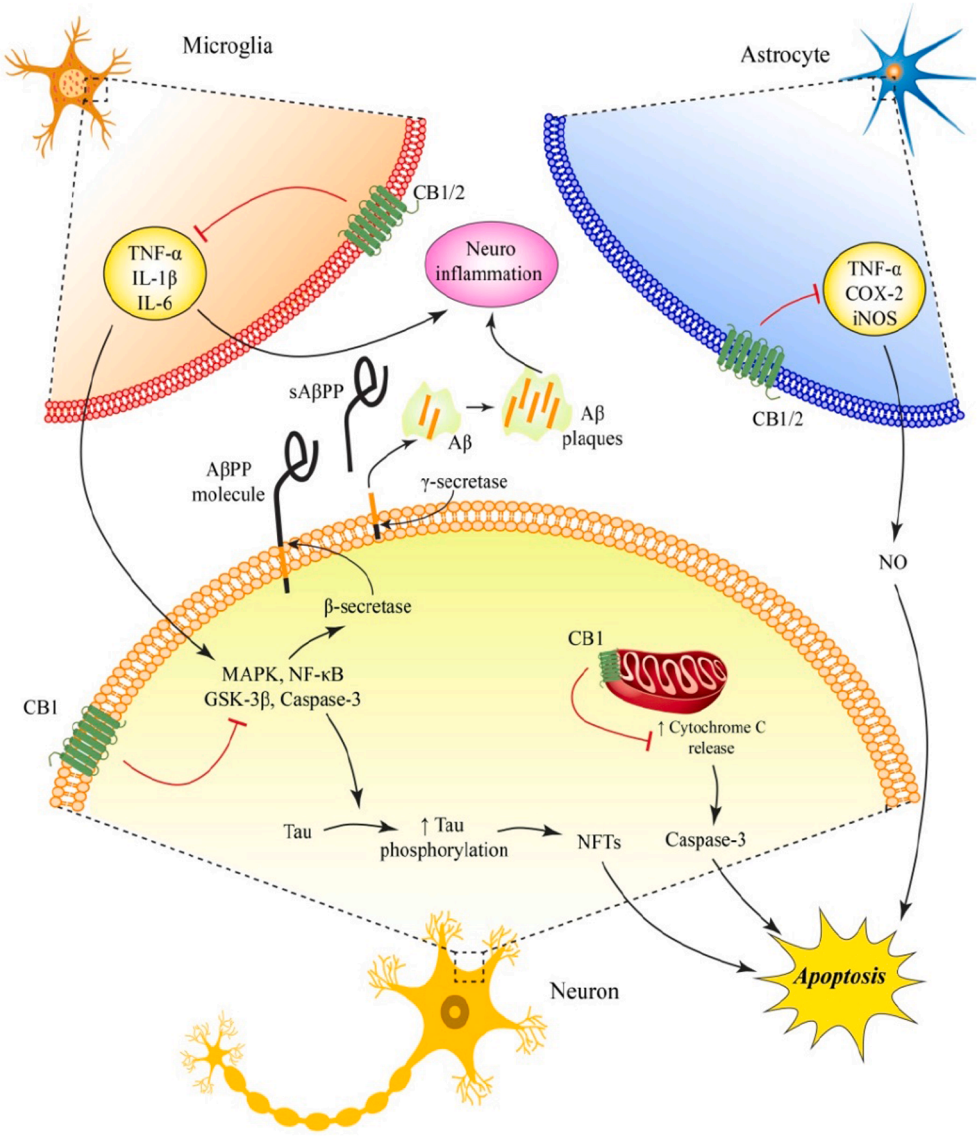

Fig. 1. Neurodegeneration signaling pathways that might be inhibited by CB_1/CB_2 activation.

protein kinase (MAPK), glycogen synthase kinase-3β (GSK-3β) and caspase-3 pathways [7–9,11] and cause neuroinflammation around Aβ plaques [13,14]; production of TNF-α, inducible nitric oxide synthase (iNOS) and cyclooxygenase-2 (COX-2) in astrocytes and consequently, nitric oxide (NO) which leads to cell death in neurons [15]; pathways of MAPK, GSK-3β and caspase-3 in neurons which lead to the emergence of Aβ monomers and NFTs [16–18]; the release of cytochrome C via mitochondria in neurons which leads to cell death [19–22].

Based on these facts, the elevation of AEA concentration in the brain through the inhibition of FAAH might be a promising avenue for AD treatment.

Catalytic triad (CT) is the main part of FAAH which comprises three residues Ser217, Ser241 and Lys142 [23]. Hydrolysis of AEA occurs in the CT through a nucleophilic attack of Ser241 on the substrate carbonyl group. Crystallography studies showed that in addition to the active site there are three cavities and channels leading away from the catalytic triad that are vital for the enzyme function [24,25]. The membrane access channel (MAC) which directs substrate to the next lipophilic pocket named acyl chain-binding pocket (ABP). The ABP accommodates the non-polar part of substrate like the lipophilic chain of AEA. Cytosolic access channel or cytosolic port (CP) is a hydrophilic channel which directs polar products from active site into the cytosol.

ACh hydrolyzing in neuronal synapses is mainly performed by AChE. Another cholinesterase known as AChE's sister is BuChE whose active site structure is very similar to that of AChE and mostly is found in the liver. On the basis of recent studies, unlike AChE, the activity of BuChE in the brain significantly increases during the disease progression [26,27].

Generally, hydrolysis of Ach occurs at the end of a deep groove of AchE called the gorge. The first place in which the initial binding of ligand occurs, is the peripheral anionic site (PAS) leading away from the catalytic triad (CT) located at the rim of the gorge [28,29]. The oxyanion hole (OH) is a hydrophobic site comprised of three residues Trp84, Ph330 and Glu99 which are thought to form π-cation interactions with quaternary ammonium group of substrates [30,31]. The main stage of hydrolysis of substrate occurs at the bottom of the gorge where the CT (Ser200, His440 andGlu327), anionic site and acyl pocket are located [32].

From two aspects, the active site structures of three enzymes described above resemble each other. all enzymes have a CT with the same nucleophile residue (Serine). There is also a hydrophobic channel (ABP) far away from the CT in FAAH which is similar to the PAS in ChEs.

In the current study, on the basis of the aforementioned facts and inspired by the structures of the native substrates, the SARs of the well-known inhibitors of these enzymes that most of them include an active carbonyl group, tertiary amine section and a lipophilic moiety and also our initially *in silico* results from structure of active sites, we designed and synthesized a new series of highly electrophilic "serine trap" carbamate based analogs **3a-q** in the hope of inhibiting both enzymes effectively (Fig. 2.). The structures of substrates and well-known FAAH /AchE inhibitors [26,27,33–38] and our four parts designed molecules are shown in Fig. 3. All target compounds were tested for their inhibitory

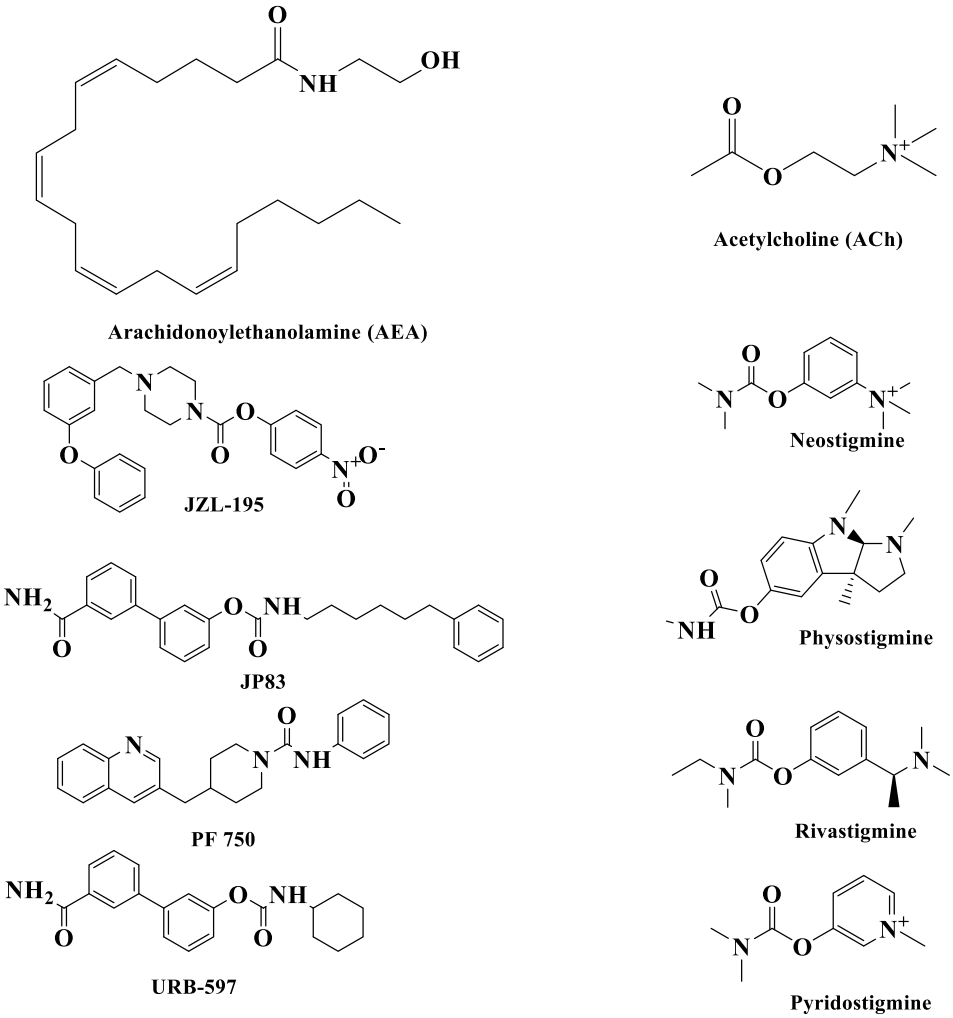

Fig. 2. Structure of native substrates and well-known FAAH /AChE inhibitors.

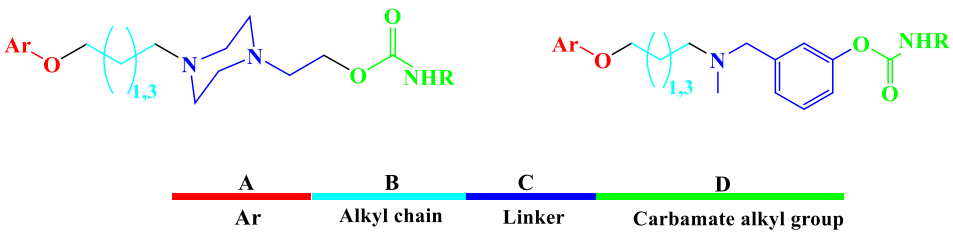

Fig. 3. Four substructures A (Aromatic rings), B (Alkyl chain), C (Linker) and D (Carbamate alkyl group) of our designed compounds as inhibitor of AChE and FAAH.

activity against FAAH and cholinesterases by employing‘ the Cayman assay kit [39] and Ellman method [40]respectively. Besides, the most potent inhibitor of both targets was chosen for investigation *in silico*, kinetic and MTT assay. Also, it was assessed for its role in improving memory in vivo, using the Morris water maze test Morris water maze.

2. Results and discussion

2.1. Synthesis

Compounds **3a-q** were synthesized as illustrated in Scheme 1.

Briefly, the hydroxyl group of heterocycles was alkylated in the presence of potassium carbonate (K_2CO_3), 1-bromo-5-chloropentane and 1-bromo-3-chloropropane to afford compounds**1a-e**. The reaction of compounds **1a-e** with 2-(piperazin-1-yl)ethan-1-ol and N,N-(3-hydroxybenzyl)-methylamine[34] in the presence of Et_3N resulted in the formation of compounds **2a-g**. Finally, in the presence of a proper base, desired carbamates **3a-q** were obtained through the nucleophilic addition of compounds **2a-g** to the corresponding isocyanates.

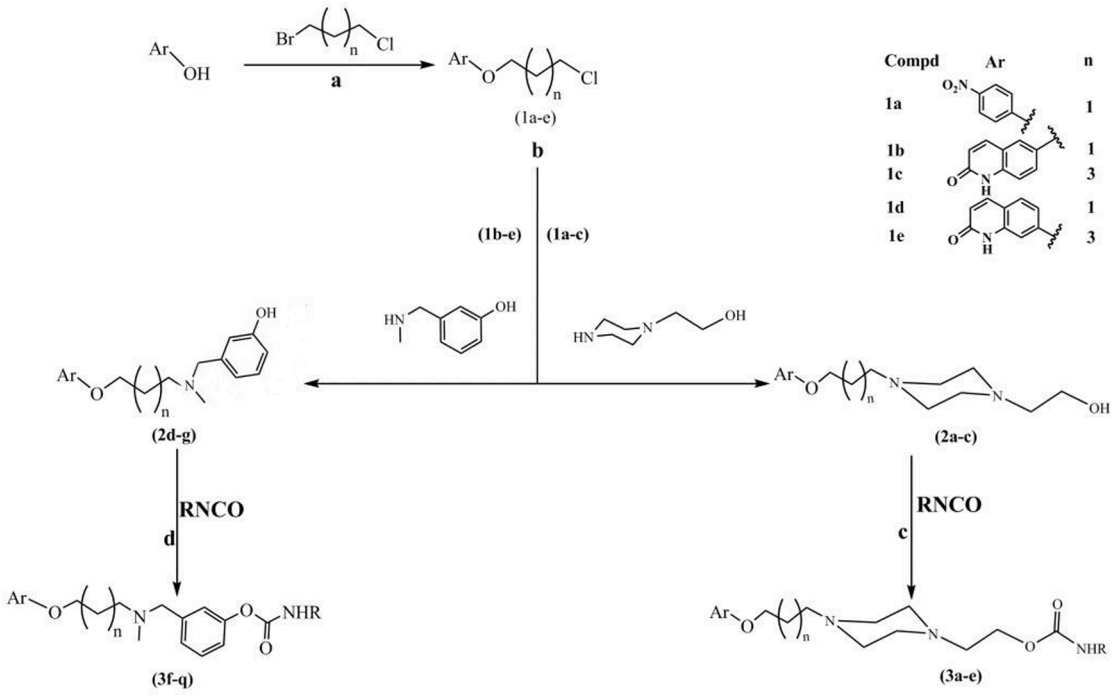

Compound	Ar	n	R
3f		1	$CH_2(CH_2)_5CH_3$
3g		1	2-Ethylhexyl
3h		1	$CH_2(CH_2)_3$-Phenyl
3i		3	$CH_2(CH_2)_5CH_3$
3j		3	2-Ethylhexyl
3k		3	$CH_2(CH_2)_3$-Phenyl
3l		1	$CH_2(CH_2)_5CH_3$
3m		1	2-Ethylhexyl
3n		1	$CH_2(CH_2)_3$-Phenyl
3o		3	$CH_2(CH_2)_5CH_3$
3p		3	2-Ethylhexyl
3q		3	$CH_2(CH_2)_3$-Phenyl

Compound	Ar	n	R
3a		1	$CH_2(CH_2)_5CH_3$
3b		1	$CH_2(CH_2)_5CH_3$
3c		1	2-Ethylhexyl
3d		3	$CH_2(CH_2)_5CH_3$
3e		3	2-Ethylhexyl

Scheme 1. Reagents and conditions: (a) K_2CO_3, acetone, reflux, 24 h; (b) ethanol, Et3N, reflux, 24 h (c) NaH, DMF, rt, 2 h; (d) Et_3N, DMSO, rt, 3 h.

2.2. Biological evaluation and structure activity studies

Different structural alterations were tried on four sections of the designed scaffold to attain a better prediction of the structural requirements needed for the activity towards enzymes. In vitro activity evaluation of all synthesized carbamates was performed by fluorescence-based Cayman FAAH inhibitor screening assay kit with the standard JZL195 [39] and Ellman method [40] with the standard inhibitor rivastigmine (Tables 1 and 2). When considering the effect of structure on activity, it is informative to examine each of the four substructures of the compounds in isolation to see how individual changes within each of these regions impact the pharmacological properties of the compounds. Our compounds dissected into four substructures A (Aromatic rings), B (Alkyl chain), C (Linker) and D (Carbamate alkyl group) (Fig. 3).

The inhibitory potential of the compounds **3a-q** extended from 0.83 ± 0.03 μM (**3i**) to ˃100 μM (**3a**) for FAAH, 0.39 ± 0.02 μM (**3i**) to 24% inhibition in 113 ± 4.8 μM (**3b**) for AChE and 1.8 ± 0.2 μM **(3i)** to 23.2 ± 3.2 μM **(3b)** for BuChE (Table S1 in supplementary data). Compound **3a** showed weak potency against FAAH (IC_{50}: ˃100 μM) and AChE (IC_{50}:75 ± 3.65 μM).

2.2.1. Alteration in section A (Aryl) and D (carbamate alkyl group)

A tiny elevation and considerable decrease of potency was observed against FAAH (IC_{50}: 88 ± 3.66 μM) and AChE (IC_{50}:˃100 μM) respectively, when the 4-phenoxy group in **3a** was replaced by 2-oxo-1,2-dihydroquinolin-6-oxy (**3b**). These activities stood almost unchanged after the *n*-heptyl gave its position to 2-ehtylhexyl (**3c**) (FAAH, IC_{50}: 90 ± 5.67 μM; AChE, IC_{50}: ˃100 μM).

2.2.2. Section B modification (alkyl chain)

For **3d** and **3e**, potency was significantly improved by elongation of propoxy to five methylene units (**3d**, FAAH, IC_{50}: 67 ± 2.22 μM; AChE, IC_{50}: 25 ± 2.23 μM), (**3e**, FAAH, IC_{50}: 70 ± 3.11 μM; AChE, IC_{50}: 11.8 ± 0.92 μM).

2.2.3. Section C (linker) modification

A dramatic increase in potency occurred when the 3-((methylamino) methyl) phenoxy was introduced instead of piperazine ethoxy applied in two previous compounds (**3i**, FAAH, IC_{50}: 0.83 ± 0.04 μM: AChE, IC_{50}: 0.39 ± 0.02 μM), (**3j**, FAAH, IC_{50}: 1.7 ± 0.11 μM; AChE, IC_{50}: 1.3 ± 0.12 μM). Inhibitory potential experienced a decline of more than eight times the rate for FAAH with substitution of 2-ethylhexyl in **3j** with phenyl butyl to afford compound **3k** (IC_{50}: 8.3 ± 0.52 μM). However, compound **3k** inactivated AChE in acceptable concentration with IC_{50} of 1.74 ± 0.25 μM.

2.2.4. Shortening the alkyl chain (section B) in three previous compounds (3i-j)

By shortening the pentoxy-moiety in the last three compounds to three methylene units, similar activity was observed for heptyl (**3f,** IC_{50}: 0.96 ± 0.07 μM) and 4-phenylbutyl (**3h**, IC_{50}: 7.5 ± 1.12 μM) carbamic substituted analogs against FAAH while 2-ethylhexyl derivative (**3g**) showed much lower activity (IC_{50}: 6 ± 0.45 μM) compared to **3j**. The inhibitory potential of the three aforementioned compounds towards AChE faced a three to nine times decrease (**3f,** IC_{50}: 2.63 ± 0.15 μM; **3g**, IC_{50}: 11.76 ± 0.38 μM; **3h**, IC_{50}: 5.97 ± 0.30 μM).

2.2.5. Replacement of aryl in section A in compounds 3f-g

The replacement of 2-oxo-1,2-dihydroquinolin-6-oxy in compounds **3f-h** with 2-oxo-1,2-dihydroquinolin-7-oxy led to compounds **3l-n** which showed the similar trend and activity against FAAH (**3l**, IC_{50}: 1.4 ± 0.03 μM; **3m**, IC_{50}: 5.7 ± 0.13 μM; 3n, 7.3 ± 0.43 μM). While *n*-heptyl carbamic substituted analog **3l** experienced a significant decrease in potency against AChE (IC_{50}: 4.82 ± 0.38 μM), 2-ethyl hexyl (**3m**) and phenylbutyl (**3n**) carbamic analogs inactivated acetylcholinesterase much more effectively as opposed to compounds **3g** and **3h** (**3m**, IC_{50}: 1.43 ± 0.16 μM; **3n**, IC_{50}: 0.92 ± 0.01 μM).

2.2.6. Elongation of alkyl chain (section B) in three previous compounds 3l-n

Finally, propoxy moiety in **3l-n** was elongated to pentoxy (**3o-q**) to observe whether they would express similar activity and trends as observed for 3**i-k**. While similar activities and trends were observed for FAAH inactivation (**3o**, IC_{50}: 1.2 ± 0.13 μM; **3p**, IC_{50}: 2.3 ± 0.16 μM; **3q**, IC_{50}: 11.3 ± 2.23 μM), **3o** and **3q** experienced nearly three times the decrease in inhibitory potency against AChE and **3p** remained almost unchanged (**3o**, IC_{50}: 1.41 ± 0.12 μM; **3p**, IC_{50}: 0.49 ± 0.51 μM; **3q**, IC_{50}: 5.91 ± 0.51 μM).

Overall, among the test inhibitors, compounds **3a-e** bearing piperazine moiety in linker section showed the weakest activity against both enzymes (Table1). A dramatic elevation in potency was observed when the piperazine moiety was replaced by 3-((methylamino) methyl)phenoxy (Table2).

As shown in Table2, in most cases *n*-heptyl carbamic substituted analogs showed more inhibitory potency compared to 2-ethylhexyl and phenylbutyl ones. For FAAH, inhibitors had a similar potency trend in the compounds with the same core and different carbamic group which was: *n*-heptyl > 2ethylhexyl > phenyl butyl.

Also, compounds containing longer alkoxy chain in section B (n = 3) were more potent against FAAH in comparison with those containing three methylene units (n = 1). Regarding the aryl groups in potent test compounds, after using 2-oxo-1,2-dihydroquinolin-6-oxy instead of 4-nitro phenoxy group in section A, a significant improvement in potency was observed. Variation also experienced another aryl, 2-oxo-1,2-dihydroquinolin-7-oxy which showed similar performance as oxo-1,2-dihydroquinolin-6-oxy.

On the other hand, no clear trend was found for AChE inactivation.

Table 1
The in vitro activities of inhibitors **3a–e** against FAAH and AChE.

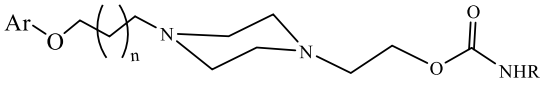

Compd	Ar	n	R	In vitro[a]	
				FAAH (μM)	AChE (μM)
3a	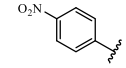	1	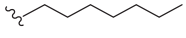	˃100	75 ± 3.65
3b		1	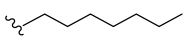	88 ± 3.66	˃100*
3c		1	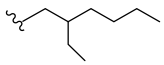	108 ± 5.67	˃100*
3d	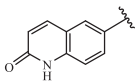	3	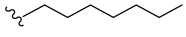	67 ± 2.22	25 ± 2.23
3e		3	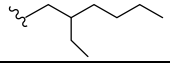	70 ± 3.11	11.8 ± 0.92

[a] IC_{50} values are expressed as the mean ± S.D. of three independent experiments.

* Inhibitory potency of **3b** and **3c** were found about 24% in 113 μM and 44% in 130 μM respectively.

2.3. Molecular docking studies

For better understanding of ligand-receptor affinity and picturing their interactions, molecular docking studies of all final compounds **3a-q** and references (JZL195 and rivastigmine) within receptors FAAH (PDB ID: 1mt5), AChE (PDB ID: 1gqr) and BuChE (PDB ID: 2wsl, Fig. S4 in supplementary data) were performed successfully using Autodock4.2

Table 2
The in vitro activities of inhibitors **3f–q** against FAAH and AChE.

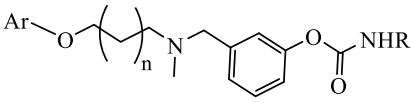

Compd	Ar	n	R	In vitro[a]	
				FAAH (μM)	AChE (μM)
3f		1	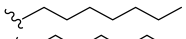	0.96 ± 0.07	2.63 ± 0.15
3g		1	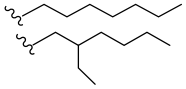	6 ± 0.45	11.76 ± 0.38
3h		1	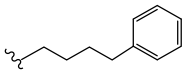	7.5 ± 1.12	5.97 ± 0.30
3i	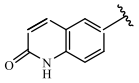	3	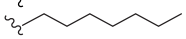	0.83 ± 0.04	0.39 ± 0.02
3j		3	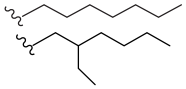	1.7 ± 0.11	1.3 ± 0.12
3k		3	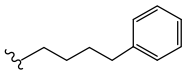	8.3 ± 0.52	1.74 ± 0.25
3l		1	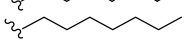	1.4 ± 0.03	4.82 ± 0.38
3m		1	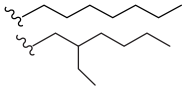	5.7 ± 0.13	1.43 ± 0.16
3n		1	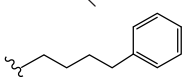	7.3 ± 0.43	0.92 ± 0.01
3o	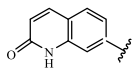	3	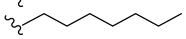	1.2 ± 0.13	1.41 ± 0.12
3p		3	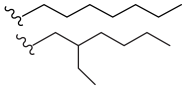	2.3 ± 0.16	0.49 ± 0.51
3q		3	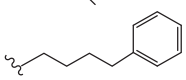	11.3 ± 2.23	5.91 ± 0.51
Rivastigmine				–	3.12 ± 0.46
JZL 195				0.0045 ± 0.0009	–

[a] IC_{50} values are expressed as the mean ± S.D. of three independent experiments.

software (http://autodock.scripps.edu/). Results were reported as binding energy (ΔG) in which high affinity was indicated by a negative score. 2D and 3D views of active site were visualized using molecular operating environment 2014.0901 (MOE) (www.chemcomp.com) and discovery studio 4.0. (www.3dsbiovia.com) respectively.

Interestingly, **3i** was stabilized through the interactions with the expected domains of AChE. As shown in Fig. 4. Trp279 (a residue in PAS) formed a π- π stacking interaction with the 2-oxo-1,2-dihydroquinolin-6-oxy group of **3i**. The cationic amine made a π-cation interaction with the benzene group of Phe330 in oxyanion hole and at the same site, the ligand affinity to AChE was improved by forming another π- π stacking interaction between the benzene groups of Trp84 and ligand's linker. Additionally, the carbamate group which potentially can form a covalent bond with Ser200, located in catalytic triad near the aforementioned residue.

Docking results also showed that the best pose of **3i** was oriented in the FAAH active site correctly as the *N*-heptyl located in the catalytic triad and cytosolic port, phenoxy and alkoxy groups together occupied the ABP and 2-oxo-1,2-dihydroquinolin-6-oxy placed in the MAC. Noticeably, the "serine trap" carbamate group formed a hydrogen bond interaction with the key Ser241 residue within the catalytic triad of FAAH (Fig. 4).

2.4. Molecular dynamic simulation

For defining dynamic interaction templates between **3i** and the enzymes, 100 ns molecular dynamic simulations were run for three targets. The 20 ns snapshots of trajectory files showed that **3i** remained in contact with the active site of enzymes during the whole 100 ns simulation period (Fig. S1, S2 and S3 in supplementary data, Fig. 5). Three main outputs of the simulations; root-mean-square derivations (RMSDs), root mean square fluctuation (RMSF) and radius of gyration (Rg) of the enzyme-inhibitor complexes were compared with the apo forms of FAAH, AChE and BuChE (Fig. S6 in supplementary data).

RMSD plot of backbone, a criterion for system stability, revealed that the complex structure of ChEs-**3i** had more stability (average $RMSD_{AChE}$: 0.151 ± 0.0153 Å; $RMSD_{BuChE}$: 0.171 ± 0.0149 Å) upon the ligand-enzyme interactions in comparison with apo-form of ChEs (average $RMSD_{AChE}$: 0.174 ± 0.023 Å; $RMSD_{BuChE}$: 0.193 ± 0.0169 Å) (Fig. 6, Fig. S6A, in supplementary data). FAAH-**3i** complex became more stable with average RMSD value of 0.187 ± 0.0219 Å relative to the apo-form with RMSD of 0.199 ± 0.0208 Å (Fig. 6).

Fig. 6 also shows RMSF as an indicator applied in molecular dynamic for macromolecule structures flexibility and local changes. Residues in/and around the active sites reached the lower amount of RMSF values indicating less flexible for these regions. RMSF values for complexes and apo-forms of AChE and BuChE (Fig. S6, B, in supplementary data) were 0.0870 ± 0.015 Å, 0.0843 ± 0.021 Å and 0.0874 ± 0.011 Å, 0.095 ± 0.016 Å respectively. These amounts for FAAH were 0.0991 ± 0.032 Å and 05.0908 ± 0.021 Å.

Radius of gyration (Rg) is a measure of protein structure compactness. **3i**-ChEs/FAAH complexes gain the higher average Rg values compared to apo-forms. Average Rg of **3i**-ChEs and **3i**-FAAH were calculated in which $Rg_{3i\text{-}AChE}$ = 2.32 ± 0.0076 Å, $Rg_{3i\text{-}BuChE}$ = 2.351 ± 0.0059 Å (Fig. S6, C, in supplementary data) and $Rg_{3i\text{-}FAAH}$ = 2.34 ± 0.0068 Å were higher than their apo-forms (FAAH 2.28 ± 0.0072 Å,

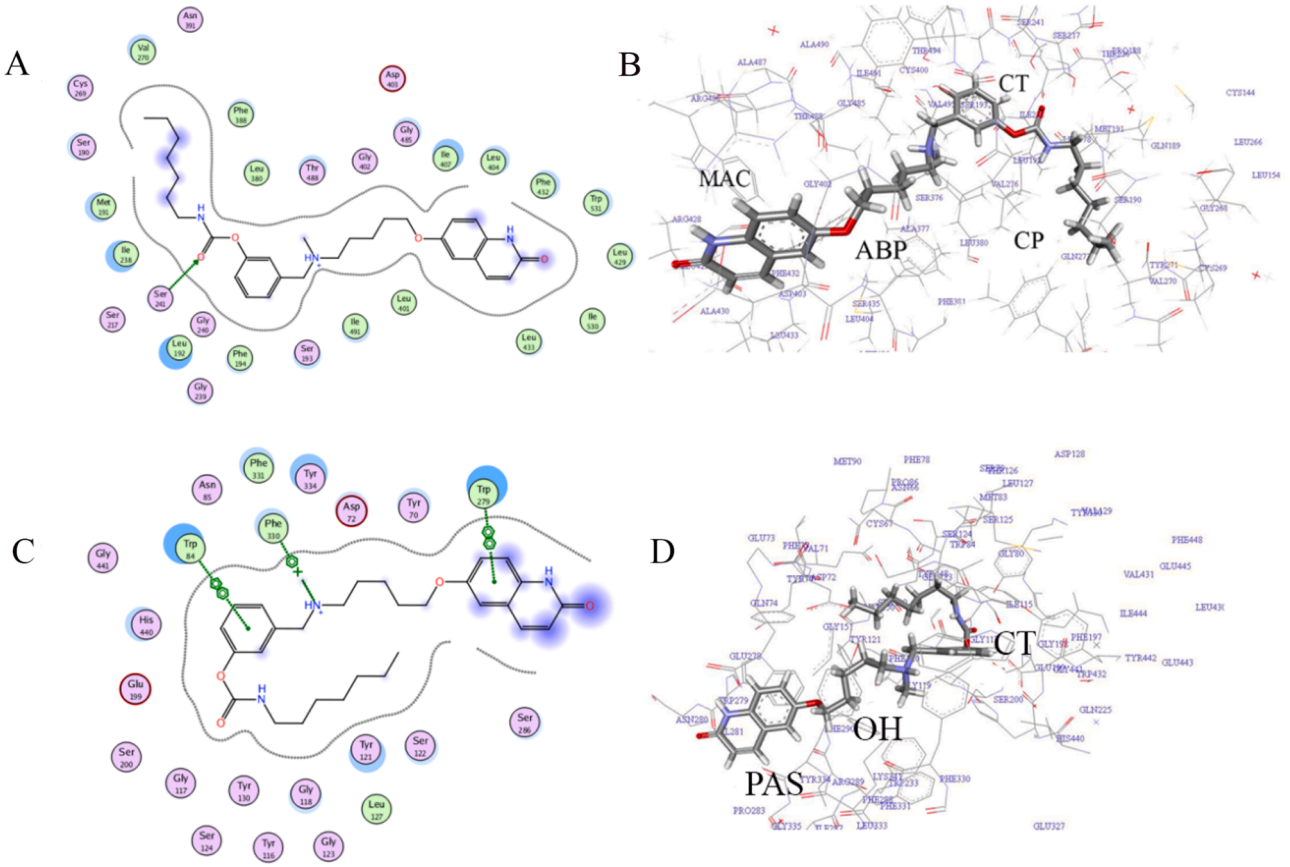

Fig. 4. 2 and 3D representation of compound **3i** interactions with FAAH and AChE. (A) 2D representation of docked **3i** within FAAH. (B) 3D illustration of **3i**-FAAH in which membrane access channel (MAC), acyl chain-binding pocket (ABP), catalytic triad (CT) and cytosolic port (CT) are defined. (C) 2D representation of **3i** docked within AChE. (D) Peripheral anionic site (PAS), oxyanion hole (OH) and catalytic triad (CT) were shown in 3D.

AChE 2.33 ± 0.0061 Å, BuChE 2.33 ± 0.0048 Å).

2.5. Cytotoxicity

Compounds **3i** also was investigated for its effects on human neuronal SH-SY5Y viability using colorimetric MTT metabolic activity assay[41] described in experimental section. We assigned 50% cell viability as the severity of the compound **3i** cytotoxic effect. As shown in Fig. 7, **3i** did not decrease SH-SY5Y cells viability until around concentration of 30 μM and showed an acceptable therapeutic window.

2.6. In vivo toxicity study

As a pointer of compound **3i**'s acute toxicity, the median lethal dose (LD_{50}) was calculated using Lorke's method [42]. Rivastigmine also was used as a reference drug. The LD_{50} dose of compound **3i** and rivastigmine was determined after intraperitoneal injection in male Wistar rats (200–250 g) and 72 h animals screening. Results indicated a low acute toxicity of compound **3i** with high LD_{50} value (42.5 ± 3.25 mg/kg) compared with rivastigmine (10.65 ± 0.95 mg/kg).

2.7. In vivo section (Morris water maze test)

Spatial learning and memory ability were evaluated by Morris water maze test [43]. The memory impairment in this model was only due to the Ach and hence did not confirm FAAH inhibition contribution.

Fig. 8. shows the escape latency time during the first 5 days of the test. On the 1st day of the test, the animals did not take anything. Obtained data showed that hyoscine injection at 1.5 mg/kg increased the time period for finding the platform relative to control group interestingly ($P < 0.001$). Also injections of rivastigmine at 2.5 mg/kg along with hyoscine, could decline latency time in a significant manner ($P < 0.05$ for 2nd day and $P < 0.001$ for days 3–5). In addition, treatment of rats with 10 and 20 mg/kg of compound **3i** decreased the latency time significantly in comparison with hyoscine group (for dose 10 mg/kg: $P < 0.05$ on the 4th day and $P < 0.01$ on the 5th day & for dose 20 mg/kg: $P < 0.01$ on the 3rd day and $P < 0.001$ on day 3–4).

In Fig. 9 the time that was spent by rats in target quadrant during probe day was depicted. Analyzed data has shown that hyoscine noticeably reduced duration of time that rats spent in target quadrant in comparison to control group ($P < 0.001$). On the other hand, co-administration of rivastigmine with hyoscine, significantly elevated this time toward hyoscine group ($P < 0.01$). Also compound **3i** treated group in doses of 10 and 20 mg/kg noteably increased the time the rats spent in the target zone compared to the hyoscine group ($P < 0.01$ and $P < 0.05$, respectively).

2.8. Cholinesterase kinetic assay

To get better insight to mechanism that compounds inhibit the enzyme, kinetic study was performed. Compound 3i the most potent compound against both cholinesterases was selected for kinetic study. The Lineweaver-Burk plot was constructed by plotting 1/vmax versus 1/[S]. According to the plot it was revealed that 3i inhibited

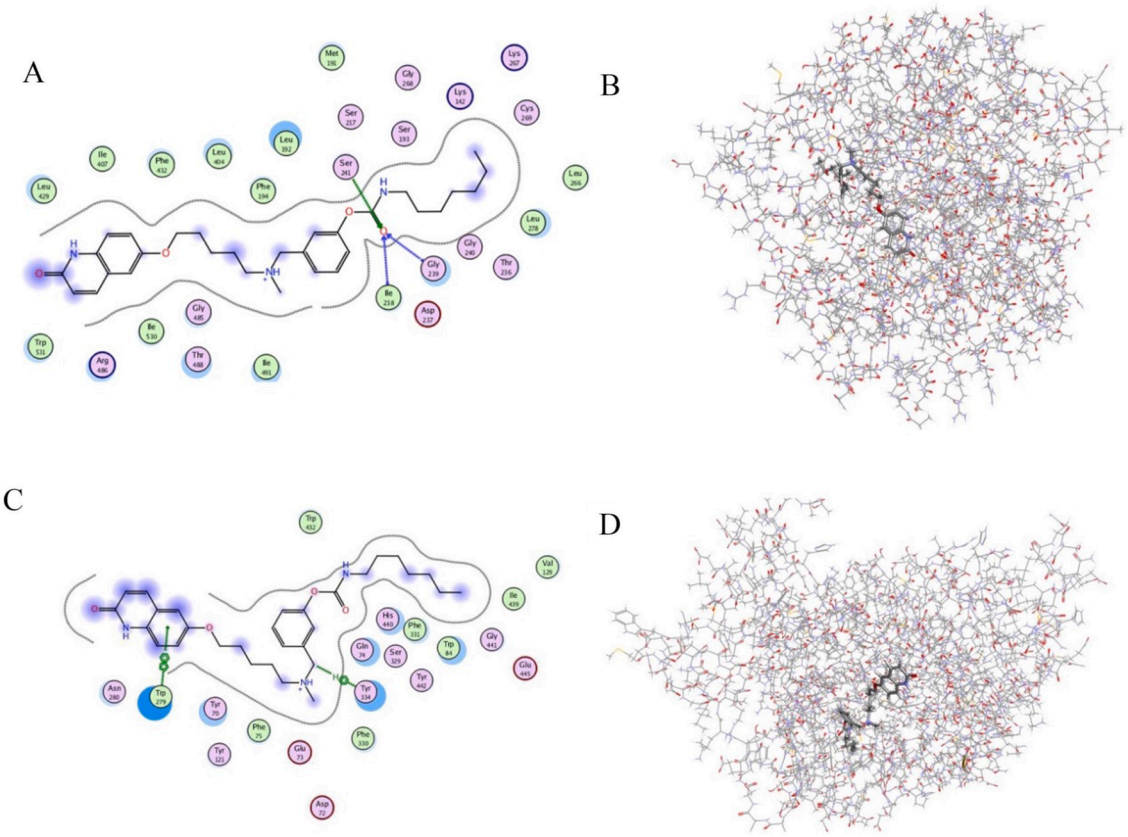

Fig. 5. (A) and (C) 2D view of **3i**-FAAH/AChE complex interactions after 100 ns simulation. (B) and (D) 3D representation of **3i** in FAAH and AChE after 100 ns.

acetylcholinesterase by mixed mode manner (Fig. 10(A)). Mixed inhibition is a type of enzyme inhibition in which the inhibitor may bind to the enzyme whether or not the enzyme has already bound the substrate but has a greater affinity for one state or the other. It was implied that 3i could interact with peripheral binding site with or without occupation of catalytic anionic site. Although in case of butyrylcholinesterase the non-competitive inhibition was revealed (Fig. 10(B)). Non-competitive inhibition is a type of enzyme inhibition where the inhibitor reduces the activity of the enzyme and binds equally well to the enzyme whether or not it has already bound the substrate. Steady-state inhibition constant (ki) of 3i for both enzymes was calculated (AChEki: 0.62, BuChEki = 0.41) using slope versus 3i concentration plots (Fig. 10C and D).

2.9. Reversibility of FAAH inhibition

Inhibition mechanism of target compounds was evaluated using preincubation method [44]. Generally, potency of an irreversible inhibitor in the presence of the FAAH prior to AMC addition is improved if the incubation times become longer. Conversely, reversible inhibitors show almost constant potency against the enzyme in different incubation times. Results of the mechanism study showed that compound **3i** blocked the enzyme in a constant manner while stronger blockage was observed by irreversible inhibitor MAFP in longer periods of incubation. (Table 3)

2.10. FAAH selectivity

The possible selectivity of two most potent compounds (**3i, 3f**) versus the other hydrolase monoacyl glycerol lipase (MAGL) also was evaluated. As shown in Table 4. **3i** and **3f** showed a promising FAAH selectivity, around 70 –fold.

3. Conclusion

In this research, a series of 17 new class of carbamate-based derivatives as inhibitors for ChEs and FAAH were designed and synthesized with respect to the structure of native substrates (AEA and acetylcholine), well-known inhibitors and tridimensional structures of enzyme binding sites. The inhibitory potency of compounds towards enzymes was investigated and compound **3i** was found to be the most potent inhibitor for three main targets (AChE, $IC_{50} = 0.39 \pm 0.02$ μM, FAAH $IC_{50} = 0.83 \pm 0.04$ μM, BuChE, $IC_{50} = 1.8 \pm 0.2$ μM). Also, **3i** exhibited memory improvement in hyoscine-induced impairment in the Morris water maze test. Furthermore, molecular docking study showed that **3i** could interact with the key residues of enzymes binding sites. In continuation of the docking study, 100 ns molecular dynamics simulation of **3i** in the enzymes active sites indicated that the compound **3i** has the ability of forming a stable ligand – receptor complex with enzymes active site. Kinetic study to understand the inhibition mechanism of ChEs via **3i** was investigated and mixed-mode manner inhibition indicated for AChE while non-competetive one revealed for BuChE.

4. Experimental section

4.1. Chemistry

All target inhibitors were characterized by ^{1}H /^{13}C NMR and mass spectra. All mass spectra were recorded on Q-trap 3200 AB SCIEX LC/MS (Framingham, USA) applying electrospray ionization (ESI) interface. ^{1}H NMR (300 MHz) and ^{13}C NMR (75 MHz) were obtained by Bruker FT-300 MHz instrument (Karlsruhe, Germany), ($CDCl_3$, DMSO-d_6). Chemical shifts were expressed in parts per million (δ) relative to the internal standard (tetramethylsilane, TMS). Perkin Elmer 1420 spectrometer (Massachuset, USA) was exploited to obtain infrared spectra applying

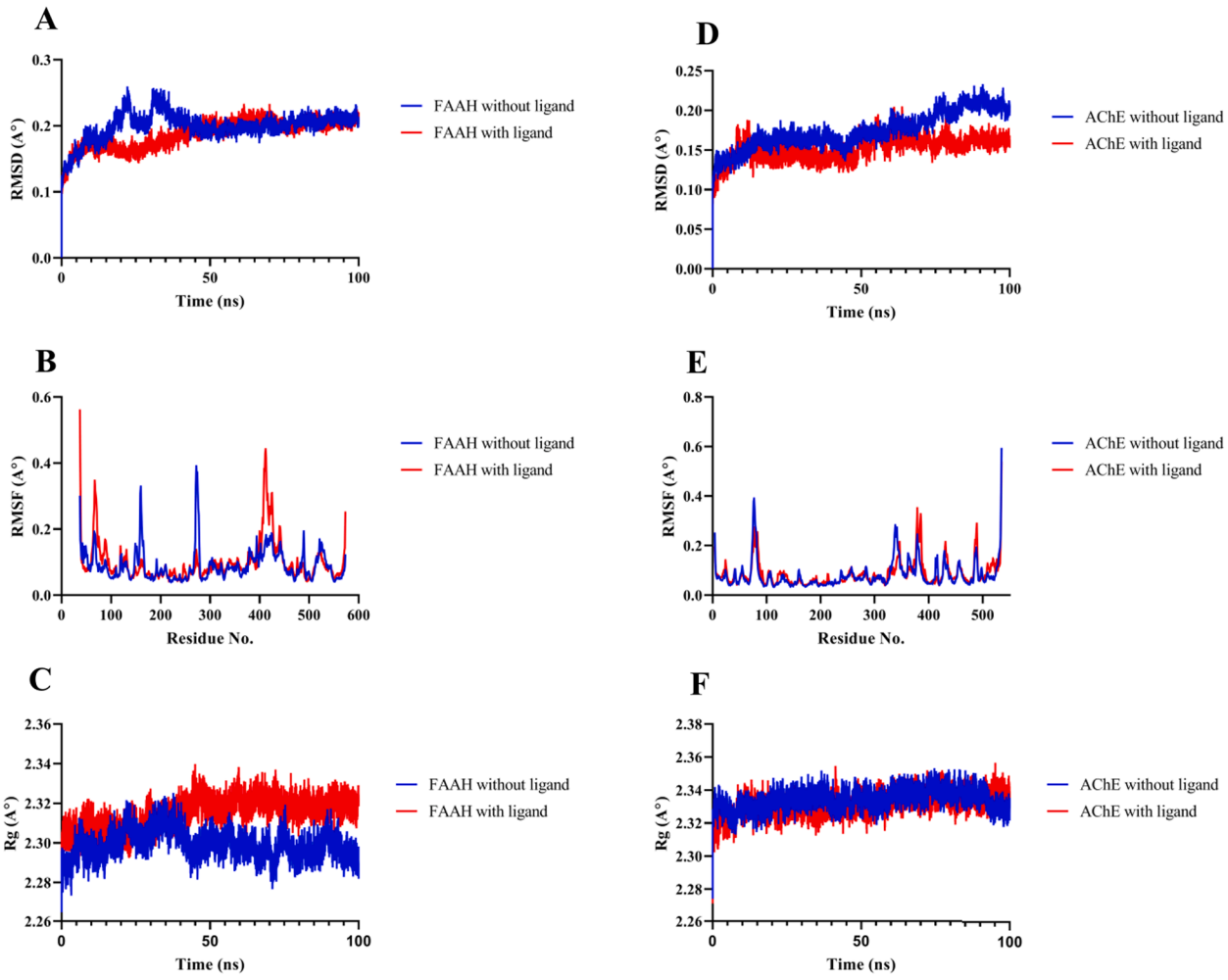

Fig. 6. (A) RMSD between FAAH with **3i** and without **3i.** (B) RMSF per residue of FAAH with and without **3i** during 100 ns simulation. (C) Rg of FAAH with **3i** and without **3i**. (D) RMSD between AChE with and without ligand. (E) RMSF per residue plot of AChE with **3i** and without **3i.** (F) Rg of AChE with **3i** and without **3i.**

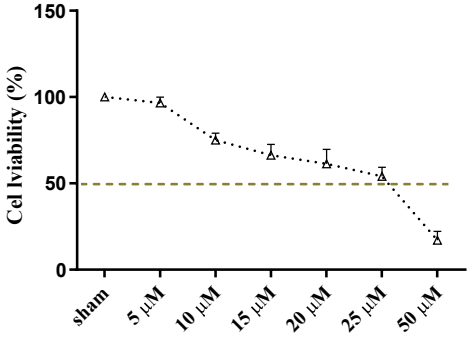

Fig. 7. Cytotoxicity of compound **3i** on human neuronal cells (SHSY-5Y) after 24 h. Data are expressed as mean ± SD (n = 8).

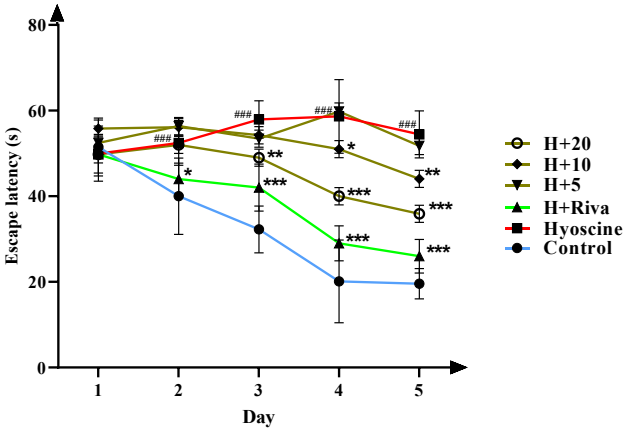

Fig. 8. The scape latency time for rats to find the hidden platform position. Hyoscine (H, 1.5 mg/kg) increased the time of finding hidden platform in comparison with control group (### P < 0.001). Pretreatment group with rivastigmine (Riva, 2.5 mg/kg) and compound **3i** diminished the scape latency time than hyoscine group (*P < 0.05, **P < 0.01 and ***P < 0.001). Data are expressed as mean ± S.D (n = 4).

KBr disks. Compounds 7-hydroxyquinolin-2(1H)-one and 6-hydroxyquinolin-2(1H)-one were obtained from Liverpool Chirochem (Liverpool, UK) and AK Scientific, Inc. (California, US) respectively. 1-Bromo-5-chloropentane was obtained from Sigma-Aldrich (UK) and 1-Bromo-3-chloropropane was purchased from Merck & Co (Darmstadt, Germany). Isocyanates was obtained from Sigma-Aldrich (USA). Thin-layer chromatography (TLC) technique was applied to monitor the progress of all reactions using aluminum precoated silica gel 60 GF-254 sheets

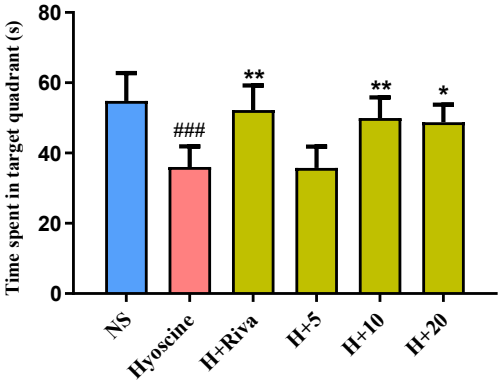

Fig. 9. The time spent in target quadrant by different group in probe day. Hyoscine (H, 1.5 mg/kg) decreased the time that spent in target quadrant in comparison with control group (### P < 0.001). Pretreatment group with rivastigmine (Riva, 2.5mh/kg) and compound **3i** increased the spent time in target quadrant than Hyoscine group (* P < 0.05 and **P < 0.01). Data are expressed as mean ± S.D (n = 4).

Merck & Co (Darmstadt, Germany). Melting points were determined with Electrothermal melting point apparatus IA9000 (Stafford, UK) and were uncorrected.

4.2. Synthesis route of compounds 1a-e and 2a-g along with their spectra are noted in the supplementary material (S.1–S.8 in supplementary data)

*4.2.1. General route to the synthesis of compounds **(3a-e)***

Sodium hydride (NaH, 0.416 mmol, 10 mg) was added to a cold solution of 2a-c (1 mmol) in tetrahydrofuran (THF, 8 ml). After 5 min respective isocyanate (2 mmol) was added into the cold solution and reaction carried on in room temperature for 2 h and finally was quenched with water (2 ml) to afford a milky suspension. The suspension was centrifuged (4 min, 350 rpm) and filtered. The crude was washed with water/ethanol (15 ml/10 ml) and after drying under vacuum was stirred in hot *n*-hexane (10 ml) for 20 min. The mixture was filtered to obtain pale yellow compounds **3a-e**.

*4.2.2. 2-(4-(3-(4-nitrophenoxy)propyl)piperazin-1-yl)ethyl heptylcarbamate **(3a)***

$C_{23}H_{38}N_4O_5$ (450.21); R_f = 0.5 (methanol); ^{1}H NMR (300 MHz, DMSO-d_6) δ (ppm) 0.88 (t, J = 6.4, 3H, —CH_3), 1.28–1.41 (m, 10*H*), 1.89–193 (m, *J* = 6.7 Hz, 2H, —CH_2—), 2.40–2.53 (m, 12H), 2.96 (q, *J* = 6.4, Hz, 2H, —$\underline{CH_2}$—NH), 4.03 (t, *J* = 5.8 Hz, 2H, —$\underline{CH_2}$—O—Ar), 4.16 (t, *J* = 6.3 Hz, 2H, —$\underline{CH_2}$—O—CO), 5.72 (t, *J* = 5.8 Hz, 1H, NH), 7.16 (d, *J* = 9.3 Hz, 2H, Ar), 8.22 (d, *J* = 9.3 Hz, 2H, Ar); ^{13}C NMR (75 MHz, DMSO-d_6) δ (ppm) 14.4, 22.5, 26.8, 29.0, 29.9, 30.6, 31.8, 53.3, 53.5, 54.6, 57.3, 60.3, 67.5, 115.5, 126.4, 141.2, 158.6, 164; (ESI, *m/z*): 451.2 $[M+1]^+$; Anal. calcd: C, 61.31; H, 8.50; N, 12.43; found: C, 61.37;

Table 3
IC_{50} values of MAFP and 3i at three different preincubation times.

Compd	5 min	30 min	60 min
MAFP	8.09 ± 0.2 nM	6.31 ± 0.1 nM	4.13 ± 0.07 nM
3i	0.98 ± 0.07 μM	0.80 ± 0.01 μM	0.85 ± 0.02 μM

Table 4
FAAH/MAGL selectivity.

Compd	FAAH IC_{50}	MAGL IC_{50}	Selectivity index
3i	0.83 ± 0.01	62.9 ± 6	75.8
3f	0.96 ± 0.07	69.4 ± 5.1	72.3

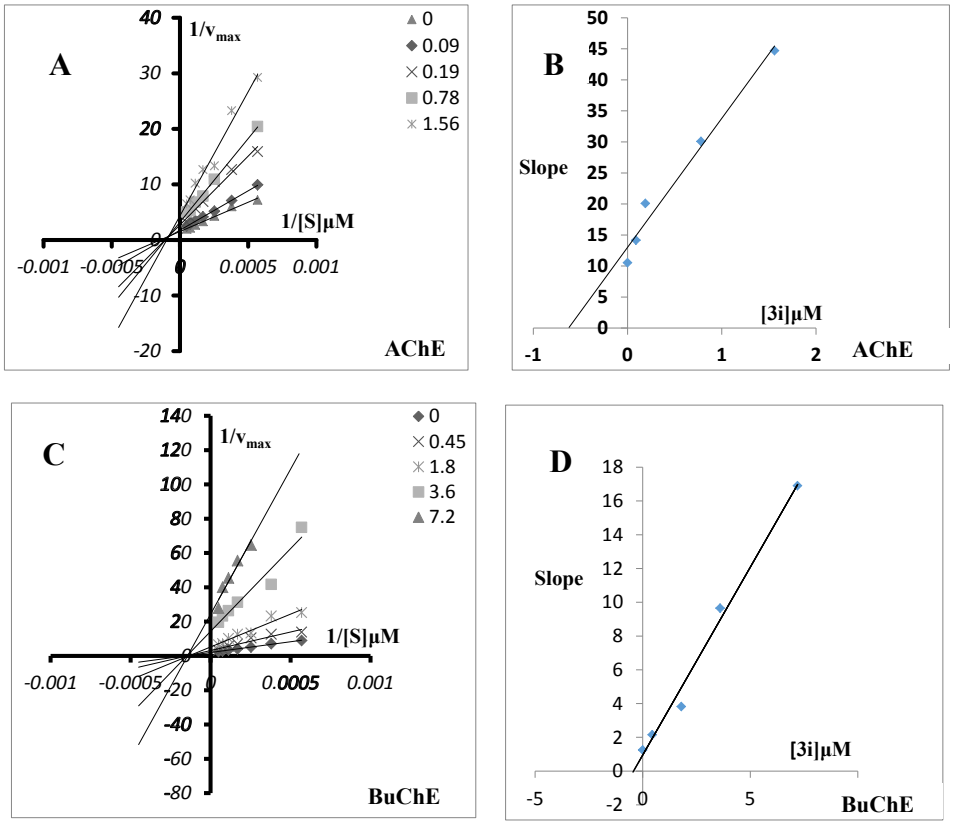

Fig. 10. (A) and (C) Lineweaver-Burk plot of AChE and BuChE inhibition by 3i at different concentration of substrate ([S]), (B) and (D) slope versus 3i concentration for calculating of K_i for AChE and BuChE.

H, 8.47; N, 12.41.

4.2.3. 2-(4-(3-((2-oxo-1,2-dihydroquinolin-6-yl)oxy)propyl)piperazin-1-yl)ethyl heptylcarbamate **(3b)**

$C_{26}H_{40}N_4O_4$ (472.3); mp: 81–84 °C; R_f = 0. 6 (methanol); ^{1}H NMR (300 MHz, DMSO-d_6) δ (ppm) 0.86 (t, J = 6.5 Hz, 3H, —CH_3), 1.24–1.41 (m, 10*H*), 1.83–1.92 (m, 2H, —CH_2—), 2.39–2.52 (m, 12H, 6 × CH_2-N), 2.95 (tq, J = 6.6 Hz, 2H, —$\underline{CH_2}$—NH), 3.99–4.05 (m, 4H, —$\underline{CH_2}$—O—Ar, —$\underline{CH_2}$—O—CO), 5.74 (t, J = 6.1, 1H, $\underline{NH}$), 6.50 (d, J = 9.5 Hz, 1H, —Ar), 7.11–7.26 (m, 3H, Ar), 7.85 (d, J = 9.6 Hz, 1H, Ar), 11.66 (s, 1H, NH-ring); ^{13}C NMR (75 MHz, DMSO-d_6) δ (ppm)14.4, 22.5, 26.7, 28.9, 29.9, 30.6, 31.7, 53.3, 53.4, 54.9, 57.2, 61.4, 66.7, 110.6, 116.8, 120.2, 120.4, 122.7, 134.2, 140.3, 153.9, 156.7, 162.0; (ESI, *m/z*): 473.2 $[M+1]^+$; Anal. calcd: C, 66.07; H, 8.53; N, 11.85; found: C, 65.90; H, 8.50; N, 11.88.

4.2.4. 2-(4-(3-((2-oxo-1,2-dihydroquinolin-6-yl)oxy)propyl)piperazin-1-yl)ethyl (2-ethylhexyl)carbamate **(3c)**

$C_{27}H_{42}N_4O_4$ (486.32); mp: 90–93 °C; R_f = 0. 55 (methanol); ^{1}H NMR (300 MHz, DMSO-d_6) δ (ppm) 0.78–0.89 (m, 6H, 2 × —CH_3), 1.18–1.28 (m, 9H), 1.86–1.91 (m, 2H, —CH_2—), 2.36–2.53 (m, 12H, 6 × CH_2—N), 2.90 (q, J = 6.1 Hz, 2H, —$\underline{CH_2}$—NH), 3.99–4.06 (m, 4H, —$\underline{CH_2}$—O—Ar, —$\underline{CH_2}$—O—CO), 5.7 (br, J = 6, 1H, $\underline{NH}$), 6.50 (d, J = 9.5 Hz, 1H, Ar), 7.09–7.28 (m, 3H, Ar), 7.85 (d, J = 9.6 Hz, 1H, Ar), 11.65 (s, 1H, NH-ring); ^{13}C NMR (75 MHz, DMSO-d_6) δ (ppm)11.1, 14.4, 21.6, 23.9, 26.7, 28.4, 30.2, 53.3, 53.4, 54.9, 57.3, 61.4, 66.7, 110.5, 116.8, 120.2, 120.3, 122.3, 133.7, 140.3, 153.9, 156.9, 162.1. (ESI, *m/z*): 487.3 $[M+1]^+$; Anal. calcd: C, 66.64; H, 8.70; N, 11.51; found: C, 66.62; H, 8.75; N, 11.45.

4.2.5. 2-(4-(5-((2-oxo-1,2-dihydroquinolin-6-yl)oxy)pentyl)piperazin-1-yl)ethyl heptylcarbamate **(3d)**

$C_{28}H_{44}N_4O4$ (500.34); mp: 90–93 °C; R_f = 0. 68 (methanol); ^{1}H NMR (300 MHz, DMSO-d_6) δ (ppm) 0.87 (t, J = 6.3 Hz,3H, —CH_3), 1.25–1.48 (m, 14H), 1.70–1.78 (m, 2H, —CH_2—), 2.24—2.53 (m, 12H, 6 × CH_2—N), 2.97 (q, J = 6.3, 2H, —$\underline{CH_2}$—NH), 3.96–4.04 (m, 4H, —$\underline{CH_2}$—O—Ar, —$\underline{CH_2}$—O—CO), 5.73 (t, J = 5.9, 1H, $\underline{NH}$), 6.50 (d, J = 9.5 Hz, 1H, Ar), 7.10–7.27 (m, 3H, Ar), 7.84 (d, J = 9.6 Hz, 1H, Ar), 11.64 (s, 1H, NH-ring); ^{13}C NMR (75 MHz, DMSO-d_6) δ (ppm)14.4, 22.5, 24.0, 26.8, 29.0, 29.1, 29.9, 30.6, 31.8, 53.3, 53.5, 57.3, 58.3, 61.4, 68.3, 110.6, 116.8, 120.2, 120.3, 122.7, 133.7, 140.3, 153.9, 158.6, 162.0; (ESI, *m/z*): 501.3 $[M+1]^+$; Anal. calcd: C, 67.17; H, 8.86; N, 11.19; found: C, 67.15; H, 8.83; N, 11.18.

4.2.6. 2-(4-(5-((2-oxo-1,2-dihydroquinolin-6-yl)oxy)pentyl)piperazin-1-yl)ethyl (2-ethylhexyl)carbamate **(3e)**

$C_{29}H_{46}N_4O_4$ (514.35); mp: 103–106 °C; R_f = 0. 65 (methanol); ^{1}H NMR (300 MHz, DMSO-d_6) δ (ppm) 0.80–0.89 (m, 6H, 2 × —CH_3), 1.16–1.50 (m, 13H), 1.70–1.79 (m, 2H, —CH_2—), 2.24–2.88 (m, 12H, 6 × CH_2—N), 2.92 (q, J = 6.1, 2H, —$\underline{CH_2}$—NH), 3.94–4.08 (m, 4H, —$\underline{CH_2}$—O—Ar, —$\underline{CH_2}$—O—CO), 5.6 (t, J = 5.8, 1H, $\underline{NH}$), 6.50 (d, J = 9.5 Hz, 1H, Ar), 7.08–7.36 (m, 3H, Ar), 7.84 (d, J = 9.6 Hz, 1H, Ar), 11.65 (s, 1H, NH-ring); ^{13}C NMR (75 MHz, DMSO-d_6) δ (ppm) 11.1, 11.8, 14.4, 23.0, 23.9, 24.0, 26.5, 28.8, 29.1, 30.6, 53.3, 53.5, 57.3, 58.3, 61.4, 68.3, 110.5, 116.8, 120.2, 120.3, 122.7, 133.7, 140.2, 154.0, 156.9, 162.0; (ESI, *m/z*): 515 $[M+1]^+$; Anal. calcd: C, 67.67; H, 9.01; N, 10.89; found: C, 67.63; H, 9.03; N, 10.91.

4.3. General route to the synthesis of compounds **(3f-q)**

To a stirring cold solution of compounds **2d-g** (1 mmol) and Et3N (1 mmol, 0.1 g) in DMSO (5 ml), DMSO solution (1.5 ml) of respective isocyanate (2 mmol) was added drop wise through the five minutes. Reaction carried on in room temperature for 7 h and finally was quenched with water (1 ml) to afford a milky suspension. The suspension was centrifuged (4 min, 350 rpm) and filtered. The crude was washed with water/ethanol (15 ml/10 ml) and after drying at vacuum was stirred in hot *n*-hexane (10 ml) for 20 min. The mixture was filtered to obtain pale yellow compounds **3f-q**.

4.3.1. 3-((methyl(3-((2-oxo-1,2-dihydroquinolin-6-yl)oxy)propyl)amino) methyl)phenyl heptylcarbamate **(3f)**

$C_{28}H_{37}N_3O_4$ (479.62); mp: 72–74 °C; R_f = 0. 65 (methanol); ^{1}H NMR (300 MHz, DMSO-d_6) δ (ppm) 0.79 (t, J = 6.1 Hz,3H, —CH_3), 1.18–1.52 (m, 10*H*), 1.87–1.96 (m, 2H, —CH_2—), 2.17 (s, 3H, N—$\underline{CH_3}$), 2.48 (t, J = 6.8 Hz, 2H, $\underline{CH_2}$NH—CH_2—Ph), 3.16 (q, J = 6 Hz, 2H, $\underline{CH_2}$—NH—CO), 3.48 (s, 2H, NH(Me) —$\underline{CH_2}$—Ph), 3.99 (t, J = 6.4 Hz, 2H, CH_2—O—Ar), 5.02 (t, J = 6, 1H, NH), 6.64 (d, J = 9.4 Hz, 1H, Ar), 6.91 (p, J = 3.3, 2.7 Hz, 2H, Ar), 7.04 (dd, J = 8.8, 2.6 Hz, 3H, Ar), 7.15–7.20 (m, 1H, Ar), 7.28 (d, J = 8.9 Hz, 1H, Ar), 7.68 (d, J = 9.5 Hz, 1H, Ar), 12.36 (s, 1H, $\underline{NH}$-ring); ^{13}C NMR (75 MHz, DMSO-d_6) δ (ppm) 14.4, 22.5, 23.8, 26.7, 27.0, 28.9, 31.7, 40.9, 42.2, 57.1, 61.6, 68.2, 99.0, 111.3, 113.7, 118.9, 120.5, 122.1, 125.4, 128.8, 129.7, 140.5, 141.1, 141.3, 151.6, 154.8, 160.2, 162.7; (ESI, *m/z*): 480.6 $[M+1]^+$; Anal. calcd: C, 70.12; H, 7.78; N, 8.76; found: C, 70.16; H, 7.75; N, 8.77.

4.4. 3-((methyl(3-((2-oxo-1,2-dihydroquinolin-6-yl)oxy)propyl)amino) methyl)phenyl (2-ethylhexyl)carbamate **(3g)**

$C_{29}H_{39}N_3O_4$ (493.29); 63–65 °C; R_f = 0. 69 (methanol);^{1}H NMR (300 MHz, DMSO-d_6) δ (ppm) 0.78–0.83 (m, 6H, 2 × —CH_3), 1.18–142 (m, 9H), 1.89–194 (m, 2H, —CH_2—), 2.17 (s, 3H, N—$\underline{CH_3}$), 2.49 (t, J = 6.8 Hz, 2H, $\underline{CH_2}$NH—CH_2—Ph), 3.11 (q, J = 6.1 Hz, 2H, $\underline{CH_2}$—NH—CO), 3.44 (s, 2H, NH(Me) —$\underline{CH_2}$—Ph), 3.98 (t, J = 6.3 Hz, 2H, $\underline{CH_2}$—O—Ar), 4.99 (t, J = 6.1, 1H, NH), 6.64 (d, J = 9.5 Hz, 1H, Ar), 6.91 (dt, J = 5.1, 2.4 Hz, 2H, Ar), 7.05 (dd, J = 9.2, 2.4 Hz, 3H, Ar), 7.14–7.21; (m, 1H, Ar), 7.28 (d, J = 8.9 Hz, 1H, Ar), 7.68 (d, J = 9.5 Hz, 1H, Ar), 12.48 (s, 1H, $\underline{NH}$-ring); ^{13}C NMR (75 MHz, DMSO-d_6) δ (ppm)11.1, 14.4, 23.0, 24.0, 25.6, 27.0, 28.8, 30.7, 42.2, 44.0, 53.7, 61.5, 66.5, 99.0, 111.3, 113.8, 118.9, 119.8, 120.5, 122.1, 125.4, 129.3, 129.7, 140.5, 141.1, 151.6, 155.0, 160.9, 162.7; (ESI, *m/z*): 494 $[M+1]^+$; Anal. calcd: C, 70.56; H, 7.96; N, 8.51; found: C, 70.59; H, 7.92; N, 8.47.

4.4.1. 3-((methyl(3-((2-oxo-1,2-dihydroquinolin-6-yl)oxy)propyl)amino) methyl)phenyl (4-phenylbutyl)carbamate **(3h)**

$C_{31}H_{35}N_3O_4$ (513.26); mp: 67–69 °C; R_f = 0. 62 (methanol);^{1}H NMR (300 MHz, DMSO-d_6) δ (ppm) 1.48–1.65 (m, 4H, 2 × —CH_2—), 1.89–1.95 (m, 2H, —CH_2—), 2.16 (s, 3H, N—$\underline{CH_3}$), 2.46–2.58 (m, 4H, $\underline{CH_2}$NH—CH_2—Ph, CH_2—$\underline{CH_2}$—Ph), 3.18 (q, J = 6.6 Hz, 2H, $\underline{CH_2}$—NH—CO), 3.43 (s, 2H, NH(Me) —$\underline{CH_2}$—Ph), 3.98 (t, J = 6.3 Hz, 2H, $\underline{CH_2}$—O—Ar), 5.01 (t, J = 6.5, 1H, NH), 6.63 (d, J = 9.4 Hz, 1H, Ar), 6.90–7.29 (m, 12H, Ar), 7.67 (d, J = 9.5 Hz, 1H, Ar), 12.37 (s, 1H, $\underline{NH}$-ring); ^{13}C NMR (75 MHz, DMSO-d_6) δ (ppm) 28.7, 28.9, 35.3, 41.6, 42.2, 53.8, 61.5, 66.7, 67.1, 110.6, 116.9, 120.2, 120.4, 120.6, 122.2, 122.7, 125.5, 126.1, 128.7, 129.3, 133.8, 140.3, 142.6, 142.7, 151.6, 154.0, 154.9, 162.1; (ESI, *m/z*): 514 $[M+1]^+$; (ESI, *m/z*): 514 $[M+1]^+$; Anal. calcd: C, 72.49; H, 6.87; N, 8.18; found: C, 72.53; H, 6.85; N, 8.15.

4.4.2. 3-((methyl(5-((2-oxo-1,2-dihydroquinolin-6-yl)oxy)pentyl)amino) methyl)phenyl heptylcarbamate **(3i)**

$C_{30}H_{41}N_3O_4$ (507); mp: 70–73 °C; R_f = 0. 67 (methanol); ^{1}H NMR (300 MHz, DMSO-d_6) δ (ppm) 0.80 (t, J = 6.1 Hz,3H, —CH_3),1.18–1.51 (m, 14H), 1.68–1.79 (m, 2H, —CH_2—), 2.11 (s, 3H, N—$\underline{CH_3}$), 2.32 (t, J = 7.0 Hz, 2H, $\underline{CH_2}$NH—CH_2—Ph), 3.16 (t, J = 6.7 Hz, 2H, $\underline{CH_2}$—NH—CO), 3.39 (s, 2H, NH(Me) —$\underline{CH_2}$—Ph), 3.90 (t, J = 6.5 Hz, 2H, $\underline{CH_2}$—O—Ar), 5.08 (t, J = 6.5, 1H, NH), 6.64 (d, J = 9.5 Hz, 1H, Ar), 6.86–7.32 (m, 7H, Ar), 7.67 (d, J = 9.5 Hz, 1H, Ar), 12.65 (s, 1H, $\underline{NH}$-ring); ^{13}C NMR (75 MHz, DMSO-d_6) δ (ppm) 14.4, 23.0, 23.0, 23.8, 24.0, 24.2, 28.8, 29.0, 31.0, 42.2, 44.0, 57.1, 61.6, 68.3, 105.7, 110.4, 116.8, 120.2, 120.3, 121.6, 122.6, 125.3, 129.2, 133.8, 140.2, 141.3, 151.7, 154.0, 155.0, 162.1; (ESI, *m/z*): 508 $[M+1]^+$; Anal. calcd: C, 75.62; H, 7.21; N, 8.02; found: C, 75.53; H, 7.18; N, 7.99.

4.4.3. 3-((methyl(5-((2-oxo-1,2-dihydroquinolin-6-yl)oxy)pentyl)amino) methyl)phenyl (2-ethylhexyl)carbamate **(3j)**

$C_{31}H_{43}N_3O_4$ (521.33); mp: 71–74 °C; R_f = 0. 7 (methanol); ^{1}H NMR (300 MHz, DMSO-d_6) δ (ppm) 0.78–83 (m, 6H, 2 × —CH_3), 1.18–1.51 (m, 13H), 1.71–1.75 (m, 2H, —CH_2—), 2.11 (s, 3H, N—CH_3), 2.32 (t, J = 6.8 Hz, 2H, CH_2NH—CH_2—Ph), 3.11 (q, J = 6.5 Hz, 2H, CH_2—NH—CO), 3.40 (s, 2H, NH(Me) —CH_2—Ph), 3.91 (t, J = 6.3 Hz, 2H, CH_2—O—Ar), 5.01 (t, J = 6.3, 1H, NH), 6.64 (d, J = 9.5 Hz, 1H, Ar), 6.87–7.32 (m, 7H, Ar), 7.67 (d, J = 9.5 Hz, 1H, Ar), 12.59 (s, 1H, NH-ring); ^{13}C NMR (75 MHz, DMSO-d_6) δ (ppm) 11.3, 14.4, 23.0, 23.0, 24.0, 27.0, 29.0, 29.1, 30.7, 31.0, 42.2, 44.0, 57.1, 61.6, 68.3, 110.5, 116.8, 120.2, 120.3, 122.0, 122.7, 125.3, 129.2, 133.8, 140.2, 141.4, 151.7, 154.0, 155.0, 158.9, 162.8; (ESI, m/z): 522 $[M+1]^+$; Anal. calcd: C, 71.37; H, 8.31; N, 8.05; found: C, 71.33; H, 8.27; N, 8.13.

4.4.4. 3-((methyl(5-((2-oxo-1,2-dihydroquinolin-6-yl)oxy)pentyl)amino) methyl)phenyl (4-phenylbutyl)carbamate **(3k)**

$C_{33}H_{39}N_3O_4$ (541.29); mp: 83–86; R_f = 0. 75 (methanol); ^{1}H NMR (300 MHz, DMSO-d_6) δ (ppm) 1.35–1.59 (m, 8H), 1.70–1.75 (m, 2H, —CH_2—), 2.11 (s, 3H, N—CH_3), 2.47–2.59 (m, 4H, CH_2NH—CH_2—Ph, CH_2—CH_2—Ph), 3.06 (q, J = 6.1, 2H, CH_2—NH—CO), 3.39 (s, 2H, NH (Me) —CH_2—Ph), 3.90 (t, J = 6.4 Hz, 2H, CH_2—O—Ar), 5.08 (t, J = 5.9, 1H, NH), 6.61 (d, J = 9.5 Hz, 1H, Ar), 6.60–7.28 (m, 12H, Ar), 7.64 (d, J = 9.5 Hz, 1H, Ar), 12.36 (s, 1H, NH-Ar); ^{13}C NMR (75 MHz, DMSO-d_6) δ (ppm) 27.0, 28.7, 29.4, 30.3, 35.3, 41.5, 42.2, 57.2, 61.6, 68.3, 110.5, 116.9, 120.2, 120.5, 122.1, 122.7, 125.4, 126.1, 128.7, 129.3, 133.8, 140.3, 141.4, 142.5, 142.7, 151.7, 154.0, 154.9, 162.1; (ESI, m/z): 542 $[M+1]^+$]$^+$; Anal. calcd: C, 73.17; H, 7.26; N, 7.76; found: C, 73.15; H, 7.28; N, 7.73.

4.4.5. 3-((methyl(3-((2-oxo-1,2-dihydroquinolin-7-yl)oxy)propyl)amino) methyl)phenyl heptylcarbamate **(3l)**

$C_{28}H_{37}N_3O_4$ (479.62); mp: 83–85 °C; R_f = 0. 6 (methanol); ^{1}H NMR (300 MHz, DMSO-d_6) δ (ppm) 0.86 (t, J = 6.1 Hz, 3H, —CH_3), 1.41–1.50 (m, 10H), 1.90–1.97 (m, 2H, —CH_2—), 2.15 (s, 3H, N—CH_3), 2.51 (t, J = 6.8 Hz, 2H, CH_2NH—CH_2—Ph), 3.05 (q, J = 6.3 Hz, 2H CH_2—NH—CO), 3.49 (s, 2H, NH(Me) —CH_2—Ph), 4.06 (t, J = 6.4 Hz, 2H, CH_2—O—Ar), 5.08 (t, J = 6, 1H, NH), 6.31 (d, J = 9.5 Hz, 1H, Ar), 6.72–6.82 (m, 1H, Ar), 6.79–6.85 (m, 2H, Ar), 6.96 (dd, J = 7.8, 2.4 Hz, 1H, Ar), 7.03 (t, J = 2.0 Hz, 1H, Ar), 7.12 (d, J = 7.6 Hz, 1H, Ar), 7.55 (d, J = 8.7 Hz, 1H, Ar), 7.69 (t, J = 5.7 Hz, 1H, Ar), 7.80 (d, J = 9.5 Hz, 1H, Ar), 11.59 (s, 1H, NH-ring); ^{13}C NMR (75 MHz, DMSO-d_6) δ (ppm)14.2, 22.8, 23.4, 24.0, 26.98, 29.0, 31.3, 42.5, 44.0, 56.2, 61.3, 68.1, 104.5, 109.4, 115.7, 119.2, 119.3, 119.4, 122.3, 122.8, 125.3, 130.2, 133.5, 140.4, 141.3, 151.5, 154.0, 155.2, 162.3; (ESI, m/z): 480.6 $[M+1]^+$; Anal. calcd: C, 70.12; H, 7.78; N, 8.76; N, 7.76; found: C, 70.16; H, 7.72; N, 8.71.

4.4.6. 3-((methyl(3-((2-oxo-1,2-dihydroquinolin-7-yl)oxy)propyl)amino) methyl)phenyl (2-ethylhexyl)carbamate **(3m)**

$C_{29}H_{39}N_3O_4$ (493.29); 63–65 °C; R_f = 0. 53 (methanol); ^{1}H NMR (300 MHz, DMSO-d_6) δ (ppm) 0.77–0.86 (m, 6H, 2 × —CH_3), 1.19–1.39 (m, 9H), 1.84–191 (m, 2H, —CH_2—), 2.19 (s, 3H, N—CH_3), 2.46 (t, J = 6.8 Hz, 2H, CH_2NH—CH_2—Ph), 3.11 (q, J = 6 Hz, 2H, CH_2—NH—CO), 3.43 (s, 2H, NH(Me) —CH_2—Ph), 3.97 (t, J = 6.1 Hz, 2H, CH_2—O—Ar), 5.37 (t, J = 5.8, 1H, NH), 6.47 (d, J = 9.4 Hz, 1H, Ar), 6.64–6.73 (m, 2H, Ar), 6.86–7.08 (m, 3H, Ar), 7.11–7.22 (m, 1H, Ar), 7.33 (d, J = 8.5 Hz, 1H, Ar), 7.63 (d, J = 9.6 Hz, 1H, Ar), 12.25 (s, 1H, NH-ring); ^{13}C NMR (75 MHz, DMSO-d_6) δ (ppm)10.8, 14.2, 22.7, 24.3, 21.7, 25.6, 27.7, 30.7, 42.0, 43.5, 51.7, 65.5, 68.3, 99.4, 113.2, 114.3, 119.2, 119.8, 120.5, 122.8, 124.6, 130.5, 132.3, 141.7, 142.3, 151.6, 155.3, 162, 163.7; (ESI, m/z): 494 $[M+1]^+$; Anal. calcd: C, 70.56; H, 7.96; N, 8.51; N, 7.76; found: C, 70.49; H, 7.95; N, 8.47.

4.4.7. 3-((methyl(3-((2-oxo-1,2-dihydroquinolin-7-yl)oxy)propyl)amino) methyl)phenyl (4-phenylbutyl)carbamate **(3n)**

$C_{31}H_{35}N_3O_4$ (513.26); mp: 67–69 °C; R_f = 0. 69 (methanol); ^{1}H NMR (300 MHz, DMSO-d_6) δ (ppm) 1.43–1.68 (m, 4H) 1.83–1.93 (m, 2H, —CH_2—), 2.27 (s, 3H, N—CH_3), 2.44–2.57 (m, 4H, CH_2NH—CH_2—Ph, CH_2—CH_2—Ph), 3.23 (q, J = 6.3 Hz, 2H, CH_2—NH—CO), 3.44 (s, 2H, NH(Me) —CH_2—Ph), 3.92 (t, J = 6.2 Hz, 2H, CH_2—O—Ar), 5.48 (t, J = 6.1 Hz, 1H), 6.68 (d, J = 9.4 Hz, 1H, Ar), 7.07–7.23 (m, 10H, Ar), 7.29–7.59 (m, 2H, Ar), 7.61 (d, J = 9.5 Hz, 1H,Ar), 12.13 (s, 1H, NH-ring); ^{13}C NMR (75 MHz, DMSO-d_6) δ (ppm) 27.0, 30.3, 34.6, 41.5, 58, 62, 67.7, 109, 117, 120.4, 120.5, 120.8, 122.3, 122.7, 125.4, 127, 129.5, 130.6 135, 144.3, 145.7, 147.8, 153.2, 156.0, 158.9, 158.7, 164.1; (ESI, m/z): 514 $[M+1]^+$; Anal. calcd: C, 72.49; H, 6.87; N, 8.18; found: C, 72.43; H, 6.83; N, 8.21.

4.4.8. 3-((methyl(5-((2-oxo-1,2-dihydroquinolin-7-yl)oxy)pentyl)amino) methyl)phenyl heptylcarbamate **(3o)**

$C_{30}H_{41}N_3O_4$ (507.3); mp: 82–84 °C; R_f = 0. 60 (methanol); ^{1}H NMR (300 MHz, DMSO-d_6) δ (ppm) 0.78 (t, J = 6.3 Hz,3H, —CH_3),1.18–1.51 (m, 14H), 1.68–1.79 (m, 2H, —CH_2—), 2.13 (s, 3H, N—CH_3), 2.31 (t, J = 6.8 Hz, 2H, CH_2NH—CH_2—Ph), 3.05 (q, J = 5.9 Hz, 2H, CH_2—NH—CO), 3.41 (s, 2H, NH(Me) —CH_2—Ph), 3.92 (t, J = 6.3 Hz, 2H, CH_2—O—Ar), 5.46 (t, J = 5.7 Hz, 1H, NH), 6.48 (d, J = 9.5 Hz, 1H, Ar), 6.68–6.95 (m, 4H, Ar), 7.09–7.22 (m, 2H, Ar), 7.34 (dd, J = 8.6, 4.0 Hz, 1H, Ar), 7.65 (d, J = 9.4 Hz, 1H, Ar), 12.44 (s, 1H, NH-ring); ^{13}C NMR (75 MHz, DMSO-d_6) δ (ppm) 11.4, 20.0, 21.0, 21.8, 22.5, 23.2, 27, 31, 31.3, 41, 44.0, 52.1, 59.3, 65.3, 100.7, 110.4, 113.8, 120.5, 120.8, 121.7, 122.8, 128.3, 129.7, 133.8, 140, 141.3, 147.5, 151.0, 152.0, 162.8; (ESI, m/z): 508 $[M+1]^+$; Anal. calcd: C, 70.98; H, 8.14; N, 8.28; found: C, 70.90; H, 8.16; N, 8.24.

4.4.9. 3-((methyl(5-((2-oxo-1,2-dihydroquinolin-7-yl)oxy)pentyl)amino) methyl)phenyl (2-ethylhexyl)carbamate **(3p)**

$C_{31}H_{43}N_3O_4$ (521.33); 82–84 °C; R_f = 0. 75 (methanol); ^{1}H NMR (300 MHz, DMSO-d_6) δ (ppm) 0.77–0.86 (m, 6H, 2 × CH_3), 1.18–1.39 (m, 13H, —CH_3, —CH_3), 2.18 (s, 3H, N—CH_3), 2.46 (t, J = 6.8 Hz, 2H, CH_2NH—CH_2—Ph), 3.11 (q, J = 6.2 Hz, 2H, CH_2—NH—CO), 3.43 (s, 2H, NH(Me) —CH_2—Ph), 3.98 (t, J = 6.3 Hz, 2H, CH_2—O—Ar), 5.38 (t, J = 6.0 Hz, 1H, NH), 6. 47 (d, J = 9.5 Hz, 1H, Ar), 6.63–7.34 (m, 7H, Ar), 7.63 (d, J = 9.5 Hz, 1H, Ar), 12.18 (s, 1H, NH-ring); ^{13}C NMR (75 MHz, DMSO-d_6) δ (ppm) 13.5, 14.2, 23.0, 23.8, 24.9, 26.0, 28.5, 29.8, 30.7, 31.8, 42.2, 44.0, 57.9, 63.6, 69.3, 112.7, 115.8, 125.2, 126.3, 128.3, 129.7, 130.3, 131.2, 133.8, 140.8, 145.6, 153.5, 154.7, 158.0, 161.9, 162.0; (ESI, m/z): 522 $[M+1]^+$; Anal. calcd: C, 70.98; H, 8.14; N, 8.28; found: C, 70.90; H, 8.16; N, 8.24.

4.4.10. 3-((methyl(5-((2-oxo-1,2-dihydroquinolin-7-yl)oxy)pentyl) amino)methyl)phenyl (4-phenylbutyl)carbamate **(3q)**

$C_{33}H_{39}N_3O_4$ (541.29); mp: 83–86; R_f = 0. 75 (methanol); ^{1}H NMR (300 MHz, DMSO-d_6) δ (ppm) 1.35–1.75 (m, 10H), 2.13 (s, 3H, N—CH_3), 2.2.47–2.59 (m, 4H, CH_2NH—CH_2—Ph, CH_2—NH—CO), 3.06 (q, J = 6.1, 2H, 2H, CH_2—NH—CO), 3.41 (s, 2H, NH(Me) —CH_2—Ph), 3.91 (t, J = 6.4 Hz, 2H,), 5.13 (t, J = 6 Hz, 1H, NH), 6.46 (d, J = 9.5 Hz, 1H, Ar), 6.88–7.28 (m, 10, Ar), 7.61 (d, J = 9.5, Ar), 12.25 (s, 1H, NH-ring); ^{13}C NMR (75 MHz, DMSO-d_6) δ (ppm) 26.4, 27.9, 30.02, 31.3, 37.5, 44.7, 45.3, 55.1, 63.3, 71.5, 114.7, 119.3, 121.5, 123.7, 125.1, 128.3, 130.7, 133.3, 136.4, 140.3, 142.5, 145.8, 146.4, 148.8, 149.2, 151.3, 156.5, 158.1, 162.0; (ESI, m/z): 542 $[M+1]^+$; Anal. calcd: C, 73.17; H, 7.26; N, 7.76; found: C, 73.11; H, 7.24; N, 7.79.

4.5. FAAH inhibition assay

In vitro Activity evaluation of all final compounds was performed by fluorescence-based Cayman FAAH inhibitor screening assay Kit (item number: 10005196) [39]. 7-amino-4-methylcoumarin-arachidonamide (AMC-AA) is hydrolyzed by the FAAH and release the fluorophore

substrate, 7-amino-4-methylcoumarin (AMC) [45,46]. By preventing AMC production through the FAAH enzyme inhibition, fluorescence of the sample falls down. Hence, the test compounds showed their inhibitory potentials (IC_{50}) by amount of decreasing in fluorescent emission originated from AMC and Inhibitory activity was analyzed in ex355-em465nm wave lengths. In summary, test solutions were prepared via dissolving compounds **3a–q** in dimethyl sulfoxide–in twelve concentrations (0.05–>100 μM) and JZL 195 was chosen as a reference. To a mixture of diluted FAAH (10 μl) and buffer (170 μl, 125 mM Tris-HCl, pH 9.0 containing 1 mM EDTA), test solutions (10 μl) were added and preincubated for five minutes at 37 °C. After adding AMC-AA (10 μl, 20 μM) to the mixtures and after 30 min incubation at 37 °C with gentle shaking, fluorescence was measured using Synergy H_4 Hybrid Multi-mode microplate reader (Biotek, Model:H_4MLFPTAD). Inhibitor and FAAH enzyme solutions were not added to the Control and blank wells respectively and each assay performed in triplicate. The method did not confirm the probable enhancement level of endogenous FAAH.

4.6. 6. Mechanism study of FAAH inhibition (reversible/irreversible)

The study was performed according to the method described above in three different incubation times 5, 30 and 60 min. Irreversible inhibitor MAFP was purchased from Enzo life sciences (France).

4.7. 7. MAGL inhibition assay

IC_{50} of the compounds were calculated using monoacylgelycreol lipase inhibitor screening assay kit from Cayman Chemical Co. In brief, MAGL hydrolazes the substrate, 4-nitrophenylacetate, to 4-nitrophenol which is traceable with an absorbance of 405–412 nm. Reactions were performed in 96 well microtiter plates with final volume of 180 μl. Three wells were taken as 100% initial activity which consisted of 150 μl of assay buffer (10 mM Tris-HCl, pH 7.2, containing 1 mM EDTA), 10 μl of MAGL containing solution, 10 μl of the solvent used for inhibitor. Blank solutions were prepared by adding 160 μl of assay buffer, 10 μl of solvent used for inhibitors. Wells of inhibitors also were filled by 150 μl of assay buffer, 10 μl MAGL and 10 μl of inhibitors solutions ranged from 0.05 to 150 μl. All aforementioned wells were incubated for 5 min prior to adding 10 μl of substrate (final concentration 150 μM). After the incubation had proceeded for 30 min, absorbance values of all wells were measured using Synergy H_4 Hybrid Multi-mode microplate reader (Biotek, Model:H_4MLFPTAD) at 408 nm. The amount of inhibition of each concentration of inhibitors were calculated using the equation

$$\left(\frac{(A(100\%initial\ \ activity) - A(inhibitor)) - A(blank\ \ solution)}{A(100\%\ \ initial\ \ activity) - A(blank\ \ solution)}\right)*100$$

Resulted sigmoidal log (dose)/ response curve was used to IC_{50} measurement using GraphPad Perism software.

4.8. ChEs inhibition assay

5,5-Dithiobis-(2-nitrobenzoic acid) (DTNB), AChE (E.C.3.1.1.7, from electrical eel, 1000 Units/mg), BuChE (E.C.3.1.1.8 BChE from equine serum), acetylthiocholine iodide, and butyrylthiocholine iodide were obtained from Sigma-Aldrich(Steinheim, Germany). Potassium dihydrogen phosphate (KH_2PO_4), dipotassium hydrogen phosphate (K2HPO4), - potassium hydroxide (KOH) and sodium hydrogen carbonate were provided by Fluka. The standard rivastigmine powder was received as a gift from Razak Pharma Ltd. (Iran).

Briefly, to prepare test solutions, target compounds were dissolved in DMSO (1 ml) and methanol (9 ml) and diluted with assay buffer (0.1 M, KH_2PO_4/K_2HPO_4, pH 8) until defined assay concentrations were reached.

Five concentrations of each target compound and rivastigmine as a reference for triplicates were tested for inhibitory potency on AChE ranged 20–80%.

Each test solution (100 ml) was added to the assay medium (0.1 M, phosphate buffer, 3 ml, pH 8; AChE 2.5 Unit/ml; 0.01 M, DTNB, 100 ml). After 15 min incubating at 25 °C on the shaker, 20 ml of the substrate (AT) was added to the assay tube. Absorbance changing was screened at 412 nm for 6 min on the baseline defined by blank (3 ml buffer, water 200 ml water, 100 ml DTNB and 20 ml substrate) via Unico Double Beam Spectrophotometer (SQ4802). Finally, inhibition curve analyzing (log [inhibitor] vs %inhibition) determined the IC_{50} values. The same method with butyrylthiocholine iodide instead of acetylthiocholine iodide was used to evaluate anti- butyrylcholinestrase activity. Probable enhancement in endogenous concentration of acetylcholine and butyrylcholine could not be investigated by Ellman method.

4.9. Molecular docking

To better understand target compounds binding mode within the enzymes, AutoDock package was used [47,48]. The PDB format of X-ray crystal structure of FAAH (PDB ID: 1mt5; in complex with inhibitor: methyl arachidonyl fluorophosphonate (MAFP); resolution: 2.8 Å),AChE (PDB ID: 1gqr; in complex with inhibitor: rivastigmine; resolution: 2.2 Å) and BuChE (PDB ID: 2wsl; in complex with inhibitor: ethyl dihydrogen phosphate; resolution: 2.00 Å) were retrieved from the Protein Data Bank (PDB). Co-crystalized small molecules (MAFP and Rivastigmine) and water molecules were removed prior to adding polar hydrogen atoms to the receptors and saving them with pdbqt format using graphical front-end AutoDock tools (1.5.6). The 2D structure of compounds **3a–q** was drawn with ChemDraw Ultra 18.0 software (http://www.cambridgesoft.com/) and 3D format was prepared using Chem3D 18.0 (http://www.cambridgesoft.com/). As estimated pKa for tertiary amines is about 11–12, the tertiary amine in all test compounds were protonated before docking. For both enzymes a grid box with a number of points of (40 × 40 × 40) along with a grid spacing of 0.375 Å was defined and the center of co-crystallized molecules were chosen as grid box center (1mt5: X = 21.536, Y = -18.472, Z = 21.139; 1gqr: X = 4.889, Y = 61.972, Z = 60.444). Genetic Algorithm Lamarckian (LGA) was taken to find the best conformations in which each job involved 100 runs. In order to view the ligand-receptor interactions, Molecular Operating Environment (MOE) version 2014.0901(www.chemcomp.com) was used to view resulting poses. Finally, compound **3i** was taken for molecular dynamic simulation.

4.10. Molecular dynamic simulation

Investigation of ligand – receptor interactions at simulated physiological condition (T = 37 °C, P = 1 atm) during 100 ns was performed using package GROMACS 4.6.3 version with charm37force field (www.gromacs.org).

Initially, enzyme structures were corrected by adding missed atoms and bonds using protein wizard of Maestro2017 [49] and the parameters needed for the ligand **3i** force field were defined by swiss param [50]. In order to neutralize the 3i-enzyme complexes 7 sodium and 4 chloride ions were added to AChE and FAAH respectively. Also, Tip3p 3-point water model was set as solvent water through the simulation. System energy was minimized with steepest-descent algorithm. Other parameters were set as described in gromacs tutorial (http://www.mdtutorials.com/gmx/complex). Results were analyzed via Visual Molecular Dynamics (VMD) [51].

4.11. Cell viability assay

Cytotoxicity of selected compounds was investigated using the colorimetric MTT metabolic activity assay. For this reason, cells were cultured in a 96-well microplate and incubated with different concentrations (5–50 μM) of synthesized compounds for 6 h. Then, cells were incubated with MTT solution (0.5 mg/ml) for 3 h. Subsequently, the

upper medium was removed and 150 µl DMSO added to each well in order to dissolve the purple crystal. To evaluate cell viability, the absorbance was measured at two wavelengths (545 nm and 630 nm as a reference) using an ELISA reader. Fig. 6. presents the correlation between different concentrations of compound X and Z and cell viability on human neuronal cells (SHSY-5Y).

4.12. 10. In vivo toxicity study

The median lethal dose (LD_{50}) of compound 3i was investigated using Lorke's method [42] and rivastigmine was selected as reference drug. Male Wistar rats in the weight range of 200–250 g were purchased from Bu Ali pharmaceutical research center, Iran, Mashhad, University of Medical Sciences. The animals were kept at room temperature (21 ± 2 °C) on a 12/12 light/dark cycle with free access to water and food. Animals were maintained and handled during experimental procedure based on the Mashhad Medical Sciences Ethics Committee Acts (code: IR.MUMS.SP.1395.67). The desired dose of compounds was mixed into a solution of %5 DMSO, normal saline (v/v). The rats were divided into seven groups of three animals for each compound and then were injected with different dose of test compound. After injection the rats were screening during 72 h to ascertain whether any symptom of acute toxicity such as salivation, convulsions and tremors may be observed. The average of the minimum killer dose (LD_{100}) and the maximum dose without mortality (LD_0) was indicated as median lethal dose (LD_{50}).

4.13. Morris water maze test

Male Wistar rats in the weight range of 200–250 g were purchased from Bu Ali pharmaceutical research center, Iran, Mashhad, University of Medical Sciences. The animals were kept at room temperature (21 ± 2 °C) on a 12/12 light/dark cycle with free access to water and food. Animals were maintained and handled during experimental procedure based on the Mashhad Medical Sciences Ethics Committee Acts (code: IR.MUMS.SP.1395.67). Morris Water Maze was used to assess hippocampal-dependent learning, including acquisition and retention of memory. The water maze consisted of a black round pool which was 136 cm in diameter and 90 cm in height and was filled to a depth of 60 cm with 22 ± 1 °C water. The pool had four equal quadrants, northeast (NE), northwest (NW), southeast (SE) and southwest (SW) that were placed in a dark room with visual signs on the room walls. A black platform (13 cm in diameter) was placed in the NW quadrant, 2 cm under the water surface. Also animal swimming paths were recorded by a camera that was located above the pool. The procedure of the test took six days. On the 1st day, animals swam to find the platform (~1 cm above the water surface) from the 4 different quadrants. Those rats who could not find the platform, were helped in finding it and they rested on it for 20 *sec*. On days 2–5, the platform was immersed under the surface and the experiment was repeated. On the 6th day (probe day), the platform was removed from the water. On probe day, all groups (except control group) received intra-peritoneal injection Hyoscine (1.5 mg). After 20 min, positive control animals were injected intraperitoneally with 5, 10, 20 mg/kg of 3i and rivastigmine 2.5 mg/kg. finally, one hour after drug injection the test was run. The duration of the trial was 60 *sec* and the rats started to swim from the farthest quadrant as opposed to the target quadrant. The path length, escape latency time and time spent in target quadrant were used to evaluate the spatial memory of animals.

4.14. Statistical analysis

Statistical analyses were done using GraphPad Prism software 8 (GraphPad, La Jolla, CA, USA). One-way ANOVA followed by Tukey as a post hoc test was applied to determine significance. P-value of <0.05 was considered significant. Data are presented as mean ± S.D and all experiments were performed in three independent experiments.

4.15. Pan-assay interference compounds (PAINS) analysis

The most potent compound 3i was filtered for PAINS assay [52] exploiting online filters http://zinc15.docking.org/patterns/apps/checker/, http://www.swissadme.ch/index.php/, and https://smartsview.zbh.uni-hamburg.de/smartssearch (center for bioanformatics of Hamburg university). None of the mentioned filters indicated 3i as PAINS.

4.16. Cholinesterase kinetic study

Mechanism of anti-cholinesterase activity of the most potent compound **3i** was investigated using Lineweaver-Burk plot (Fig. 10). Compound 3i was prepared in four concentrations (0.09, 0.19, 0.78, 1.56 µM for AChE; 0.45, 1.8, 3.6, 7.2 µM for BuChE). Six different concentrations of substrate (*S* acetylthiocholine iodide, butyrylthiocholine iodide reciprocal) (20000, 13000, 6000, 4000, 2600, 1755 µM) were also used to draw the 1/Vmax versus 1/[S] plots. Another plot used for inhibition constant (ki) was drawn using slope of each curve of Lineweaver-Burk plot versus **3i** concentrations. The intercept of the horizontal axis was defined as ki.

Author contributions

The manuscript was written through contributions of all authors.

Declaration of Competing Interest

The authors declare that they have no known competing financial interests or personal relationships that could have appeared to influence the work reported in this paper.

Acknowledgment

We are grateful to Research deputy of Mashhad University of Medical Sciences for financial support of this research (grant no.950922). This work was part of Ph.D thesis of Mahdi Faal Maleki.

Appendix A. Supplementary material

Supplementary data to this article can be found online at https://doi.org/10.1016/j.bioorg.2021.104684.

References

[1] G. Bedse, A. Romano, A.M. Lavecchia, T. Cassano, S. Gaetani, The role of endocannabinoid signaling in the molecular mechanisms of neurodegeneration in Alzheimer's disease, J. Alzheimers Dis. 43 (4) (2015) 1115–1136.
[2] C.L. Masters, D.J. Selkoe, Biochemistry of amyloid beta-protein and amyloid deposits in Alzheimer disease, Cold Spring Harb. Perspect. Med. 2 (6) (2012) a006262.
[3] J. Avila, Tau phosphorylation and aggregation in Alzheimer's disease pathology, FEBS Lett. 580 (12) (2006) 2922–2927.
[4] A. Contestabile, The history of the cholinergic hypothesis, Behav. Brain Res. 221 (2) (2011) 334–340.
[5] J.A. Fernandez, L. Rojo, R.O. Kuljis, R.B. Maccioni, The damage signals hypothesis of Alzheimer's disease pathogenesis, J. Alzheimers Dis. 14 (3) (2008) 329–333.
[6] T.C. Frank-Cannon, L.T. Alto, F.E. McAlpine, M.G. Tansey, Does neuroinflammation fan the flame in neurodegenerative diseases? Mol. Neurodegener. 4 (2009) 47.
[7] J. Ehrhart, D. Obregon, T. Mori, H. Hou, N. Sun, Y. Bai, T. Klein, F. Fernandez, J. Tan, R.D. Shytle, Stimulation of cannabinoid receptor 2 (CB2) suppresses microglial activation, J. Neuroinflammation 2 (2005) 29.
[8] J. Koppel, V. Vingtdeux, P. Marambaud, C. d'Abramo, H. Jimenez, M. Stauber, R. Friedman, P. Davies, CB 2 receptor deficiency increases amyloid pathology and alters tau processing in a transgenic mouse model of Alzheimer's disease, Mol. Med. 20 (1) (2014) 29–36.
[9] T.E. Saez, M. Pehar, M. Vargas, L. Barbeito, R.B. Maccioni, Astrocytic nitric oxide triggers tau hyperphosphorylation in hippocampal neurons, Vivo 18 (3) (2004) 275–280.

[10] S.-Y. Ren, Z.-Z. Wang, Y. Zhang, N.-H. Chen, Potential application of endocannabinoid system agents in neuropsychiatric and neurodegenerative diseases—focusing on FAAH/MAGL inhibitors, Acta Pharmacol. Sin. 1–9 (2020).
[11] L. Brunetti, A. Laghezza, F. Loiodice, P. Tortorella, L. Piemontese, Combining fatty acid amide hydrolase (FAAH) inhibition with peroxisome proliferator-activated receptor (PPAR) activation: a new potential multi-target therapeutic strategy for the treatment of Alzheimer's disease, Neural Regen. Res. 15 (1) (2020) 67.
[12] D. Dow-Edwards, L. Silva, Endocannabinoids in brain plasticity: Cortical maturation, HPA axis function and behavior, Brain Res. 1654 (Pt B) (2017) 157–164.
[13] B.G. Ramírez, C. Blázquez, T.G. del Pulgar, M. Guzmán, M.L. de Ceballos, Prevention of Alzheimer's disease pathology by cannabinoids: neuroprotection mediated by blockade of microglial activation, J. Neurosci. 25 (8) (2005) 1904–1913.
[14] A.M. Martín-Moreno, D. Reigada, B.G. Ramírez, R. Mechoulam, N. Innamorato, A. Cuadrado, M.L. de Ceballos, Cannabidiol and other cannabinoids reduce microglial activation in vitro and in vivo: relevance to Alzheimer's disease, Mol. Pharmacol. 79 (6) (2011) 964–973.
[15] A.M. Martín-Moreno, B. Brera, C. Spuch, E. Carro, L. García-García, M. Delgado, M. A. Pozo, N.G. Innamorato, A. Cuadrado, M.L. de Ceballos, Prolonged oral cannabinoid administration prevents neuroinflammation, lowers β-amyloid levels and improves cognitive performance in Tg APP 2576 mice, J. Neuroinflammation 9 (1) (2012) 8.
[16] X. Chen, J. Zhang, C. Chen, Endocannabinoid 2-arachidonoylglycerol protects neurons against β-amyloid insults, Neuroscience 178 (2011) 159–168.
[17] N.G. Milton, Anandamide and noladin ether prevent neurotoxicity of the human amyloid-β peptide, Neurosci. Lett. 332 (2) (2002) 127–130.
[18] M. Haghani, M. Shabani, M. Javan, F. Motamedi, M. Janahmadi, CB1 cannabinoid receptor activation rescues amyloid β-induced alterations in behaviour and intrinsic electrophysiological properties of rat hippocampal CA1 pyramidal neurones, Cell. Physiol. Biochem. 29 (3–4) (2012) 391–406.
[19] P. Zaccagnino, A. Corcelli, M. Baronio, M. Lorusso, Anandamide inhibits oxidative phosphorylation in isolated liver mitochondria, FEBS Lett. 585 (2) (2011) 429–434.
[20] C. Velez-Pardo, M. Jimenez-Del-Rio, S. Lores-Arnaiz, J. Bustamante, Protective effects of the synthetic cannabinoids CP55, 940 and JWH-015 on rat brain mitochondria upon paraquat exposure, Neurochem. Res. 35 (9) (2010) 1323–1332.
[21] P. Zaccagnino, S. D'Oria, L.L. Romano, A. Di Venere, A.M. Sardanelli, M. Lorusso, The endocannabinoid 2-arachidonoylglicerol decreases calcium induced cytochrome c release from liver mitochondria, J. Bioenerg. Biomembr. 44 (2) (2012) 273–280.
[22] G. Catanzaro, C. Rapino, S. Oddi, M. Maccarrone, Anandamide increases swelling and reduces calcium sensitivity of mitochondria, Biochem. Biophys. Res. Commun. 388 (2) (2009) 439–442.
[23] M. Mileni, S. Kamtekar, D.C. Wood, T.E. Benson, B.F. Cravatt, R.C. Stevens, Crystal structure of fatty acid amide hydrolase bound to the carbamate inhibitor URB597: discovery of a deacylating water molecule and insight into enzyme inactivation, J. Mol. Biol. 400 (4) (2010) 743–754.
[24] M. Mileni, D.S. Johnson, Z. Wang, D.S. Everdeen, M. Liimatta, B. Pabst, K. Bhattacharya, R.A. Nugent, S. Kamtekar, B.F. Cravatt, Structure-guided inhibitor design for human FAAH by interspecies active site conversion, Proc. Natl. Acad. Sci. U.S.A. 105 (35) (2008) 12820–12824.
[25] M.H. Bracey, M.A. Hanson, K.R. Masuda, R.C. Stevens, B.F. Cravatt, Structural adaptations in a membrane enzyme that terminates endocannabinoid signaling, Science 298 (5599) (2002) 1793–1796.
[26] S. Montanari, L. Scalvini, M. Bartolini, F. Belluti, S. Gobbi, V. Andrisano, A. Ligresti, V. Di Marzo, S. Rivara, M. Mor, Fatty acid amide hydrolase (FAAH), acetylcholinesterase (AChE), and butyrylcholinesterase (BuChE): networked targets for the development of carbamates as potential anti-Alzheimer's disease agents, J. Med. Chem. 59 (13) (2016) 6387–6406.
[27] R.K. Tripathi, S.R. Ayyannan, Exploration of dual fatty acid amide hydrolase and cholinesterase inhibitory potential of some 3-hydroxy-3-phenacyloxindole analogs, Archiv der Pharmazie 353 (9) (2020) 2000036.
[28] Y. Bourne, P. Taylor, P. Marchot, Acetylcholinesterase inhibition by fasciculin: crystal structure of the complex, Cell 83 (3) (1995) 503–512.
[29] M. Işık, The binding mechanisms and inhibitory effect of intravenous anesthetics on AChE in vitro and in vivo: kinetic analysis and molecular docking, Neurochem. Res. 44 (9) (2019) 2147–2155.
[30] J. Kua, Y. Zhang, A.C. Eslami, J.R. Butler, J.A. McCammon, Studying the roles of W86, E202, and Y337 in binding of acetylcholine to acetylcholinesterase using a combined molecular dynamics and multiple docking approach, Protein Sci. 12 (12) (2003) 2675–2684.
[31] E.J. Fogle, J.F. Marlier, A. Stillman, X. Gao, Y. Rao, L.I. Robins, An investigation into the butyrylcholinesterase-catalyzed hydrolysis of formylthiocholine using heavy atom kinetic isotope effects, Bioorg. Chem. 65 (2016) 57–60.
[32] A. Ordentlich, D. Barak, C. Kronman, N. Ariel, Y. Segall, B. Velan, A. Shafferman, Functional characteristics of the oxyanion hole in human acetylcholinesterase, J. Biol. Chem. 273 (31) (1998) 19509–19517.
[33] J.Z. Long, D.K. Nomura, R.E. Vann, D.M. Walentiny, L. Booker, X. Jin, J.J. Burston, L.J. Sim-Selley, A.H. Lichtman, J.L. Wiley, Dual blockade of FAAH and MAGL identifies behavioral processes regulated by endocannabinoid crosstalk in vivo, Proc. Natl. Acad. Sci. U.S.A. 106 (48) (2009) 20270–20275.
[34] K. Ahn, D.S. Johnson, L.R. Fitzgerald, M. Liimatta, A. Arendse, T. Stevenson, E. T. Lund, R.A. Nugent, T.K. Nomanbhoy, J.P. Alexander, Novel mechanistic class of fatty acid amide hydrolase inhibitors with remarkable selectivity, Biochemistry 46 (45) (2007) 13019–13030.
[35] M. Mor, S. Rivara, A. Lodola, P.V. Plazzi, G. Tarzia, A. Duranti, A. Tontini, G. Piersanti, S. Kathuria, D. Piomelli, Cyclohexylcarbamic acid 3 '-or 4 '-substituted biphenyl-3-yl esters as fatty acid amide hydrolase inhibitors: synthesis, quantitative structure−activity relationships, and molecular modeling studies, J. Med. Chem. 47 (21) (2004) 4998–5008.
[36] A. Rampa, A. Bisi, P. Valenti, M. Recanatini, A. Cavalli, V. Andrisano, V. Cavrini, L. Fin, A. Buriani, P. Giusti, Acetylcholinesterase inhibitors: synthesis and structure−activity relationships of ω-[N-Methyl-N-(3-alkylcarbamoyloxyphenyl)-methyl] aminoalkoxyheteroaryl derivatives, J. Med. Chem. 41 (21) (1998) 3976–3986.
[37] D.S. Johnson, C. Stiff, S.E. Lazerwith, S.R. Kesten, L.K. Fay, M. Morris, D. Beidler, M.B. Liimatta, S.E. Smith, D.T. Dudley, Discovery of PF-04457845: a highly potent, orally bioavailable, and selective urea FAAH inhibitor, ACS Med. Chem. Lett. 2 (2) (2011) 91–96.
[38] D. Garzinsky, S. Zahov, M.E. Voundi, W. Hanekamp, M. Lehr, Tetrazolylpropan-2-ones as inhibitors of fatty acid amide hydrolase: studies on structure-activity relationships and metabolic stability, Eur. J. Med. Chem. 160 (2018) 183–192.
[39] S. Jaiswal, R.K.P. Tripathi, S.R. Ayyannan, Scaffold hopping-guided design of some isatin based rigid analogs as fatty acid amide hydrolase inhibitors: synthesis and evaluation, Biomed. Pharmacother. 107 (2018) 1611–1623.
[40] G.L. Ellman, K.D. Courtney, V. Andres Jr, R.M. Featherstone, A new and rapid colorimetric determination of acetylcholinesterase activity, Biochem. Pharmacol. 7 (2) (1961) 88–95.
[41] M. Kianfar, A. Nezami, S. Mehri, H. Hosseinzadeh, A.W. Hayes, G. Karimi, The protective effect of fasudil against acrylamide-induced cytotoxicity in PC12 cells, Drug Chem. Toxicol. 1–7 (2018).
[42] D. Lorke, A new approach to practical acute toxicity testing, Arch. Toxicol. 54 (4) (1983) 275–287.
[43] M. Ghanbarabadi, M. Iranshahi, S. Amoueian, S. Mehri, V.S. Motamedshariaty, S. A. Mohajeri, Neuroprotective and memory enhancing effects of auraptene in a rat model of vascular dementia: experimental study and histopathological evaluation, Neurosci. Lett. 623 (2016) 13–21.
[44] T. Tuccinardi, C. Granchi, F. Rizzolio, I. Caligiuri, V. Battistello, G. Toffoli, F. Minutolo, M. Macchia, A. Martinelli, Identification and characterization of a new reversible MAGL inhibitor, Bioorg. Med. Chem. 22 (13) (2014) 3285–3291.
[45] A. Paul, D.A. Kendall, S.P. Alexander, A spectrophotometric assay for fatty acid amide hydrolase suitable for high-throughput screening, Biochem. Pharmacol. 69 (8) (2005) 1187–1193.
[46] S.J. Wilson, T.W. Lovenberg, A.J. Barbier, A high-throughput-compatible assay for determining the activity of fatty acid amide hydrolase, Anal. Biochem. 318 (2) (2003) 270–275.
[47] O. Trott, A.J. Olson, AutoDock Vina: improving the speed and accuracy of docking with a new scoring function, efficient optimization, and multithreading, J. Comput. Chem. 31 (2) (2010) 455–461.
[48] G.M. Morris, R. Huey, W. Lindstrom, M.F. Sanner, R.K. Belew, D.S. Goodsell, A. J. Olson, AutoDock4 and AutoDockTools4: automated docking with selective receptor flexibility, J. Comput. Chem. 30 (16) (2009) 2785–2791.
[49] G.M. Sastry, M. Adzhigirey, T. Day, R. Annabhimoju, W. Sherman, Protein and ligand preparation: parameters, protocols, and influence on virtual screening enrichments, J. Comput. Aided Mol. Des. 27 (3) (2013) 221–234.
[50] V. Zoete, M.A. Cuendet, A. Grosdidier, O. Michielin, SwissParam: a fast force field generation tool for small organic molecules, J. Comput. Chem. 32 (11) (2011) 2359–2368.
[51] W. Humphrey, A. Dalke, K. Schulten, VMD: visual molecular dynamics, J. Mol. Graph. 14 (1) (1996) 33–38.
[52] J.B. Baell, G.A. Holloway, New substructure filters for removal of pan assay interference compounds (PAINS) from screening libraries and for their exclusion in bioassays, J. Med. Chem. 53 (7) (2010) 2719–2740.